UNIVERSITA' DEGLI STUDI DI MILANO

Corso di Dottorato in

Ricerca Biomedica Integrata

XXXII Ciclo

Functional characterization of new SCN5A mutations associated with different patterns of arrhythmia

Tutor**:** Prof. Mirko Baruscotti

Coordinator: Prof.ssa Chiarella Sforza

Dott. Anthony Frosio

Matr. R11788

Anno Accademico 2018-2019

INDEX

PREFACE

During my three years of Ph.D. studies, I have been mainly involved in two projects regarding the role of pathological mutations of cardiac voltage-gated sodium channel ($Na_v1.5$) that are found in patients affected by different cardiac diseases.
In this initiatory part I will briefly summarize the two projects in order to give an idea of what I have done in these three years of work.

1. Functional characterization of a novel SCN5A mutation associated with Brugada syndrome.

Brugada syndrome (BrS) is a cardiac disorder characterized by conduction abnormalities that can lead to sudden death; syncope and cardiac arrest are clinical manifestations which are often associated with an enhancement of the vagal activity (Brugada et al., 2014). Mutations in the SCN5A gene ($Na_v1.5$ channel) are the most common cause of the inherited forms of BrS (Kapplinger et al., 2010).
The objective of our work was to characterize the functional behavior of mutant $Na_v1.5$ channels expressing a novel heterozygous mutation (S805L) recently identified in an Italian family affected by the BrS, using HEK293 cell as experimental model to express both Wild-Type and mutant model
When compared to the WT current, the S508L mutation significantly decreases the peak current density by 65% for the Homo condition and by 35% for the Hetero condition. Densitometric analysis carried out on western blot data further support the conclusion that S805L channels are less abundant in the plasma membrane. We also observed that the S805L mutation positively shifts the half inactivation voltage of both Homo and Hetero currents. A positive shift of the half activation voltage was also observed but only in the Homo condition. The kinetics of recovery from inactivation and the amplitude of the late sodium current were also evaluated but they were unaffected by the mutation.
In the Hetero condition, the S805L mutation causes a reduction in the channel expression, however, the positive shift of the inactivation curve suggests an increase in Na channel availability. We thus believe that the precise quantitative balance between these two phenomena and their relationship with vagal activity may underlie the clinical manifestation of the disease.

2. Biophysical study of a SCN5A compound mutation found in a child with sinus node dysfunction, atrial flutter, and drug induced long-QT syndrome.

A two-year-old patient was hospitalized for severe bradycardia and recurrent atrial flutter at Azienda Ospedaliera Papa Giovanni XXIII (Bergamo). Different treatments were performed in order to stabilize the patient and to find the right therapy (DeFilippo et al., 2014).
Several months after the first hospitalization, the medical team decided to implant a pacemaker. Focusing on the genotype of the patient, they found a compound heterozygous mutation in the SCN5A gene: K1578N was carried by the father and G1866fs by the mother. Since there are no evidences in literature that demonstrate the isoform switch of cardiac voltage-gated sodium channel, we decided to perform the experiments using the neonatal clone of the channel that presents few differences compared to the adult (for more details, view M&M). We decided to transfect HEK 293 cells with the three mutations carried by the family and verify the alterations provoked. Both parents' mutation induced a current density reduction although they do not present a pathological phenotype. K1578N/ G1866fs compound mutation had a strong impact on current density, indeed it caused a reduction of about 60% compared to the WT. Kinetic analysis revealed a robust positive shift of the voltage-dependence of activation of 9 mV and also a positive shift of inactivation curve of 5 mV, while parent's mutations do not alter these parameters. All this indicates the severe loss-of-function nature of the mutation and more experiments are obviously needed to try to explain the mechanism of action that underlies the pathology.

GENERAL INTRODUCTION

The Heart

Anatomy and functions

The heart is a muscular, hollow, and unequal organ that lays in the anterior mediastinum, behind the body of the sternum and above the diaphragm (**Figure1**). It works as a pump, pumping blood through the circulatory system around the entire body. The pericardium, a double-membraned connective sac, surrounds the heart and attaches it to the mediastinum.

The heart has a pyramidal shape with the basis facing upward, to the right and the apex downward, to the left. Its axis is therefore oblique so that a third of it lies to the right of the median plane and two thirds of it to the left.

It consists of four chambers: the upper two are called atria and are separated by the interatrial septum, while the lower two are called ventricles and are separated by the interventricular septum. Atria and ventricles are isolated from each other by means of the atrioventricular septum. The only way for the blood to flow from top to bottom chambers of the organ involves the atrioventricular valves: the tricuspid valve allows a monodirectional blood flow from the right atrium to the right ventricle, and the mitral (or bicuspid) valve allows the same type of blood flow from the left atrium to the left ventricle.

The heart is made up of three tissues: endocardium, myocardium, and epicardium. Endocardium is an endothelial tissue and it is the innermost layer, the myocardium is a muscular tissue constituted by striated muscle cells, and the epicardium is a connective tissue and it is the inner membrane of the pericardium.

We consider the heart "the pump" of our body in order to provide a continuous blood flow to the whole body. Blood provides the body with oxygen and nutrients, as well as assists in the removal of metabolic wastes.

The left side of the heart contains oxygenated blood, while the right side the deoxygenated one. Interatrial and interventricular *septi* prevent the blood-s mixture. Moreover, the atrioventricular valves, placed between *atria* and ventricles, and the semilunar valves, at the entrance of arteries, prevent any retrograde flow. In the right *atrium*, deoxygenated blood is collected from the superior and the inferior *venae cavae*. The blood then flows through the tricuspid valve to the right ventricle and finally through the pulmonary valve to the pulmonary trunk which branches to

provide the pulmonary circulation to the lungs. In this circuit blood exchanges carbon dioxide for oxygen through the process of respiration. After that, oxygenated blood reaches the left atrium by means of the pulmonary veins, enters the left ventricle passing the mitral valve and it is finally distributed to all tissues through the *aorta*, via the systemic circulation.

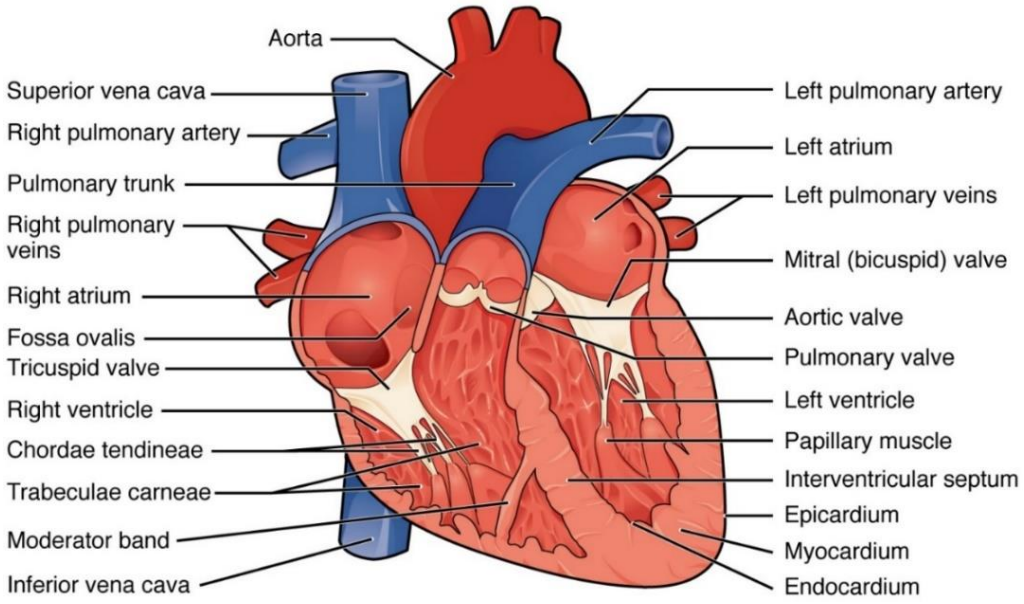

Figure 1. Anatomy of the heart.
This anterior view of the heart shows the four chambers, the major vessels and their early branches, as well as the valves. The presence of the pulmonary trunk and aorta covers the interatrial septum, and the atrioventricular septum is cut away to show the atrioventricular valves (Pinterest.com).

Cardiac muscle

Cardiac cells are mainly divided in two major types: working myocytes and conduction myocytes. The working myocytes constitute the *working myocardium,* that represents the majority of the structure and it generates the contractility that pumps blood, while the conduction myocytes make up the *conduction system,* that it is capable of generating and conducting electric impulse through the organ. The electric impulse follows a specific path thus allowing the whole heart to contract efficiently and in a coordinated way.

The conduction system of the heart

The cardiac conduction system (**Figure 2**) is a specialized structure, that is made up of particular cells able to spontaneously generate and transfer the electric impulse to the working myocardium of the various chambers of the heart.

The cardiac conduction system includes several specific regions, such as the sinoatrial node (SAN), the atrioventricular node (AVN), the bundle of His, the two bundle branches and the Purkinje fibers.

Cardiac rhythm is established in the SAN, a highly specialized group of cells located in the wall of the right atrium, where the superior *vena cava* enters the right *atrium*, since it has the highest inherent rate of depolarization. For this reason, it is also known as the natural pacemaker of the heart. From the SAN the impulse spreads to the *atria* through the internodal pathways and reaches the AVN. Here the impulse is decelerated and then reaches the bundle of His, that is divided into right and left branches, which continue with the Purkinje fibers within the ventricular walls. These fibers allow the synchronized contraction of the ventricles.

The impulse, generated by the SAN and transmitted through the heart, is called action potential.

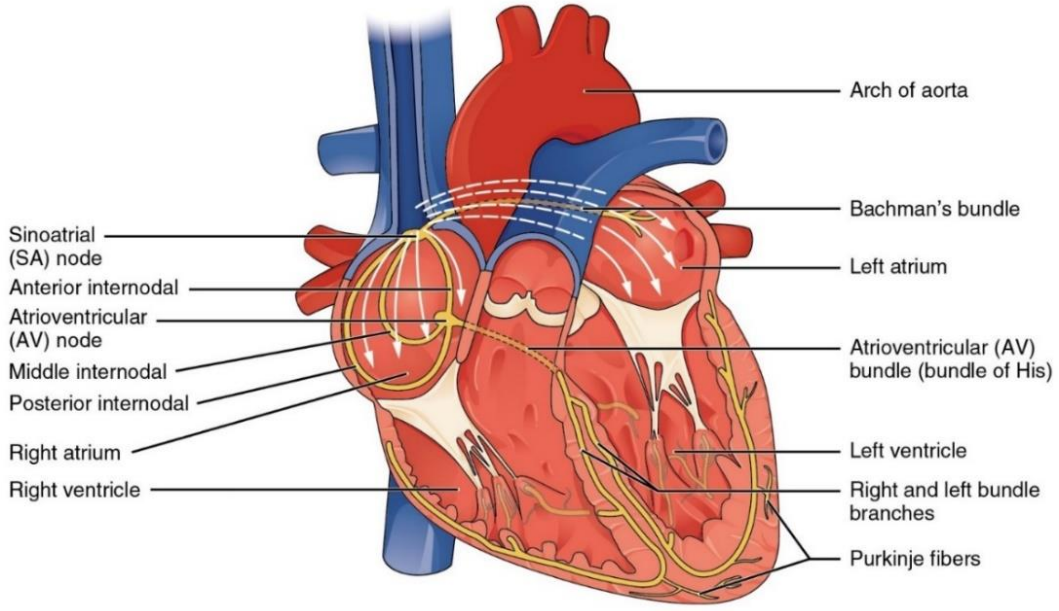

Figure 2. The conduction system of the heart.
Specialized conducting components of the heart include the sinoatrial node (SAN), the internodal pathways, the atrioventricular node (AVN), the bundle of His, the right and left bundle branches, and the Purkinje fibers (Pinterest.com).

Autonomic innervation of the heart

Heart rate is regulated by the two branches of the autonomic nervous system (ANS, **Figure 3**), the sympathetic nervous system (SNS) and the parasympathetic nervous system (PNS).

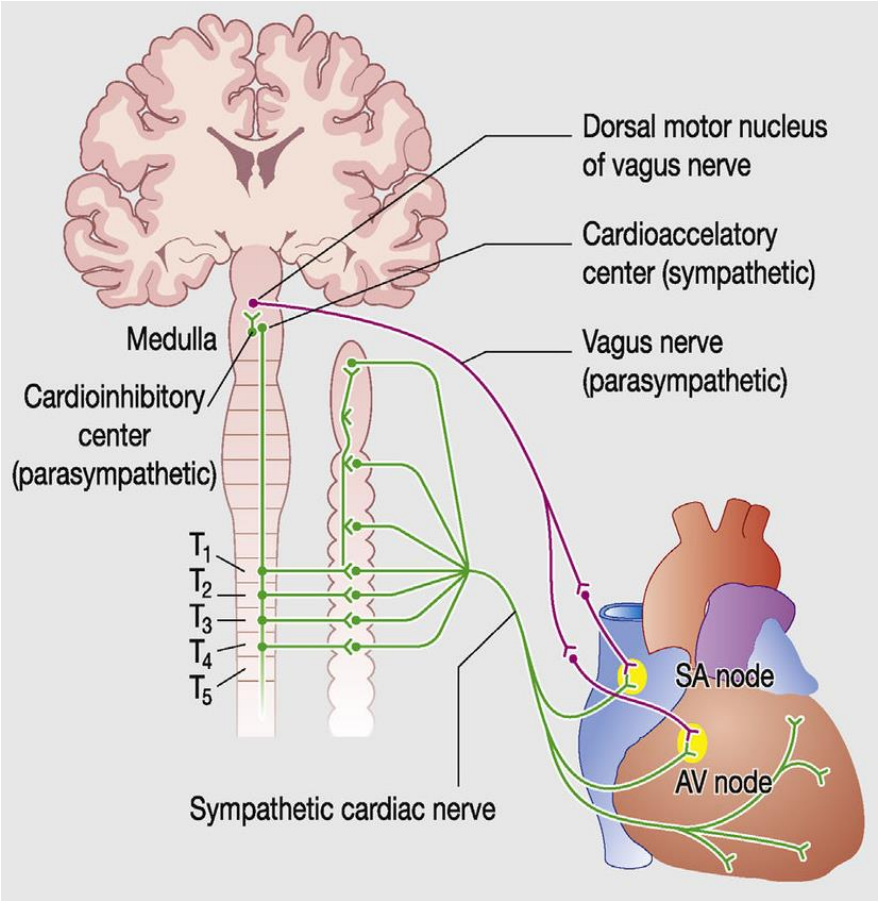

Figure 3. Autonomic innervation of the heart.
The sympathetic system innervates the whole heart, while the parasympathetic system mainly innervates the SAN and AVN (ResearchGate.net, Philippe Chevalier).

Sympathetic fibers originate from the spinal cord (T1-T4 region), contact the paravertebral ganglia and innervate SAN, *atria* and ventricles. SNS performs its functions releasing catecholamines (epinephrine and norepinephrine) and the activation of SNS causes an increase of:

1) heart rate (positive chronotropic effect);
2) power of contraction of both *atria* and ventricle (positive inotropic effect);
3) speed of conduction of the electrical impulse (positive dromotropic effect) (Brodde e Michel 1999).

Catecholamines induce depolarization of the membrane due to an increased influx of sodium and calcium ions.

Parasympathetic fibers originate from the brainstem and directly reach the SAN and AVN via vagal nerve (X cranial nerve) (Kent et al.,1974). The effects of PNS are opposite to those of SNS, inducing a decrease of:

1) heart rate (negative chronotropic effect);
2) AVN fibers excitability, slowing down the impulse transmission (negative dromotropic effect) (Brodde e Michel, 1999).

The PNS release acetylcholine, which induces hyperpolarization of the fibers' membrane due to a rapid efflux of potassium ions. Due to this action the SAN resting potential becomes more negative and therefore, more time is needed to reach the threshold of excitation. While in the AVN the hyperpolarization of the membrane causes a delay in impulse conduction.
The neurotransmitters released by the ANS binds specific membrane receptors in target tissues. All these adrenergic (mediator of SNS) and muscarinic (mediator of PNS) receptors are G-protein coupled receptors.
Noradrenaline is released from sympathetic presynaptic terminals, binds to β2-receptors and this determines an increase in the production of the intracellular cAMP (cyclic adenosine monophosphate) concentration by adenylate cyclase, a process mediated by a stimulatory Gs protein.
On the other hand, acetylcholine is released from parasympathetic presynaptic terminals and binds M2-muscarinic receptors inducing a decrease in the intracellular cAMP concentration. cAMP acts as a second messenger increasing the activity of the Protein Kinase A (PKA) which, in turn, phosphorylates several proteins on the membrane, such as the L-type Ca^{2+} channels (Walsh e Van Patten,1994; Kaumann e Molenaar,1997). In addition, cAMP increases the opening chance of HCN channels by direct binding to them in a PKA-independent way (DiFrancesco e Tortora, 1991). Phosphodiesterases (PDE) lowers the cAMP concentration by converting it to 5-AMP, thus reducing several currents, such as the I_{CaL} and the I_f current.

The action potential

The action potential is a rapid and reversible change of the electrical potential difference across the plasma membrane of excitable cells due to a sequence of ion fluxes through specialized ion channels. It represents the base for information processing, propagation and transmission.
Action potentials occur in various excitable animal cells, such as neurons (cell-to-cell communication), muscle cells (contraction) and endocrine cells (hormone release), as well as in some plant cells.
At cardiac level, the shape of the action potential varies according to the cell type and depends on both the expression and the properties of ion channels (Nerbonne & Kass., 2005); we can mainly group them in two types:

1) "fast response" (**Figure 4**), peculiar of atrial and ventricular myocardium;
2) "slow response" (**Figure 5**), found in sinoatrial node and atrioventricular node.

"Fast response" action potential

The working myocardium cells do not have spontaneous activity therefore the action potential is generated after the arrival of a stimulus coming from the sinus node cells. Fast response action potential has a duration of 200/300 ms.
Figure 4 shows the action potential of ventricular cardiomyocyte. The process can be divided into five distinct phases:

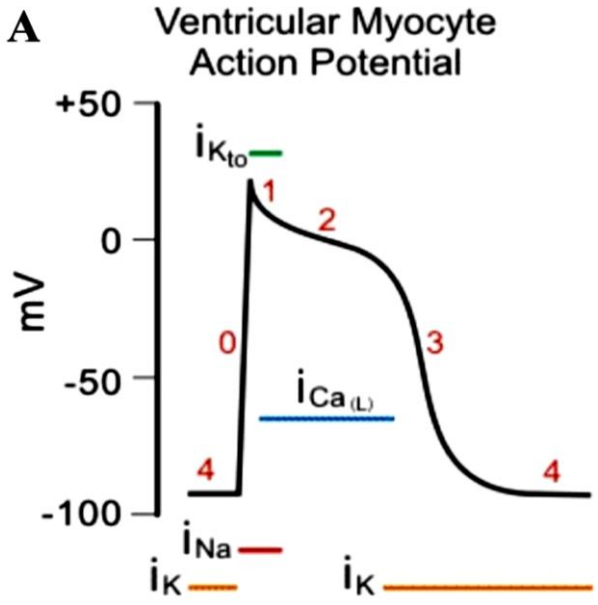

Figure 4. Schematic representation of an action potential from a working myocardium cell (cvphysiology.com/Arrhythmias).

Phase 0: it is a rapid depolarization phase, due to the quick inflow of a depolarizing sodium (Na^+) current from voltage-gated Na^+ channels;

Phase 1: it is a partial repolarization phase, caused by two main events: the activation of a potassium (K^+) transient outward current ($I_{K_{to}}$) and the voltage-dependent inactivation of voltage-gated Na^+ channels;

Phase 2: also known as the plateau phase, it is characteristic of this cell type. Here, an inward L-type calcium (Ca^{2+}) current ($I_{Ca_{(L)}}$) counteracts the transient outward K^+ current, maintaining the membrane potential between 0 and -10 mV;

Phase 3: as the $I_{Ca_{(L)}}$ stops, a series of inward K^+ currents (I_{Kur}, a very rapid current peculiar of the atrial myocytes, I_{Kr}, a fast current and I_{Ks}, a slow current) repolarize the cell to the resting potential;

Phase 4: during this phase the cell membrane potential is maintained at the resting voltage of about -80 mV mostly due to an inward K^+ current named I_{K1}. Resting state is preserved until another electrical stimulus brings up the voltage to the threshold for the activation of voltage-gated Na^+ channels.

The main difference between atrial and ventricular action potential lies in the duration of the plateau phase: this step is indeed shorter or even absent in atrial myocytes. The discrepancy arises from the different contraction power cells must generate. Ca^{2+} inflow in the plateau phase is extremely relevant in order to generate the process of Calcium-Induced Calcium Release (CICR) which is, in turn, fundamental for the physical contraction. Once Ca^{2+} ions are carried inside the plasma membrane, they bind to the Ryanodine Receptors (RYRs) located in the Sarcoplasmic Reticulum (SR) leading to a massive release of other Ca^{2+} ions. Four of these ions then bind their specific spots on troponin C causing the removal of tropomyosin from the binding site of actin to myosin that are now able to link each other: the sarcomeric contraction can now take place. At the end of the process, Sarcum Endoplasmic Reticulum Calcium-ATPase (SERCA) pumps located on the membrane of the sarcoplasmic membrane employ ATP in order to carry Ca^{2+} ions from the cytosol back to their location in the SR.

"Slow response" action potential

Since SAN cells can generate spontaneous and rhythmic beats, their action potential lacks a stable resting phase. Moreover, unlike working myocytes whose task is to contract, SAN cells have to generate and transmit the electrical impulse, so their action potential lacks the plateau phase, too. This is due to the presence of different ion channels' pattern, compared to the working myocardium. In this process three main phases occur (**figure 5**):

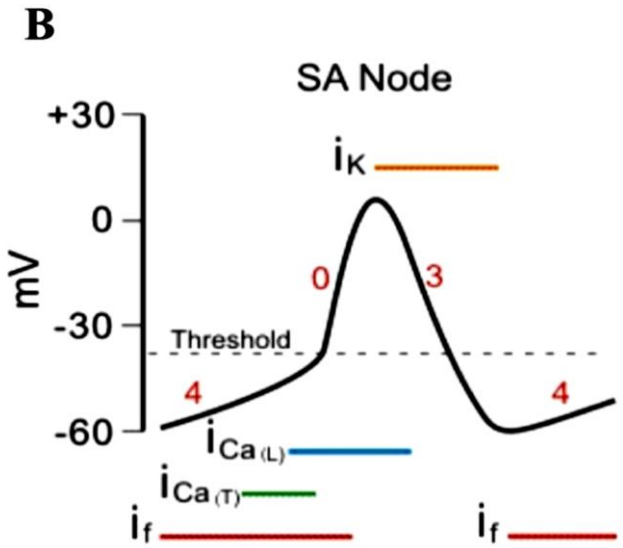

Figure 5. Schematic representation of an action potential from a working myocardium cell (cvphysiology.com/Arrhythmias).

Phase 0: it is the main depolarization phase, led by the $I_{Ca_{(L)}}$ current. Cations inflow depolarize the cell;

Phase 3: the voltage is hyperpolarized by a combination of outward K^+ currents, such as the I_{Kr} and the I_{Ks}. Furthermore, type-L Ca^{2+} channels inactivate and switch to their closed-state. The K^+ currents of this phase stop at the beginning of the following one (phase 4);

Phase 4: at the end of the repolarization phase (phase 3), the membrane potential reaches the Maximum Depolarization Point (MDP), defined as the most negative value reached during the entire cycle, at about -60 mV. In this range of voltage, Hyperpolarization activated Cyclic Nucleotide gated channels (HCN) begin to open, conducting a mixed inward current of Na^+ and K^+, the so-called funny current (I_f) (DiFrancesco et al., 1986). This peculiar current is the driving force of this phase, that is also known as the slow diastolic depolarization phase of the pacemaker cells. The membrane potential rises until the activation threshold for the type-L Ca^{2+} channels is reached, and a new depolarization phase begins (phase 0).

The electrocardiogram

The electrical activity of the heart can be recorded by electrodes placed on the skin. The electrocardiogram (**Figure 6**) is the graphic reproduction of the electrical activity of the heart during its functioning and, therefore, it is an indicator of the succession of cardiac events. By analyzing the parameters (shape, amplitude and duration) of the graph it is possible to evaluate the electrical functionality of the heart.

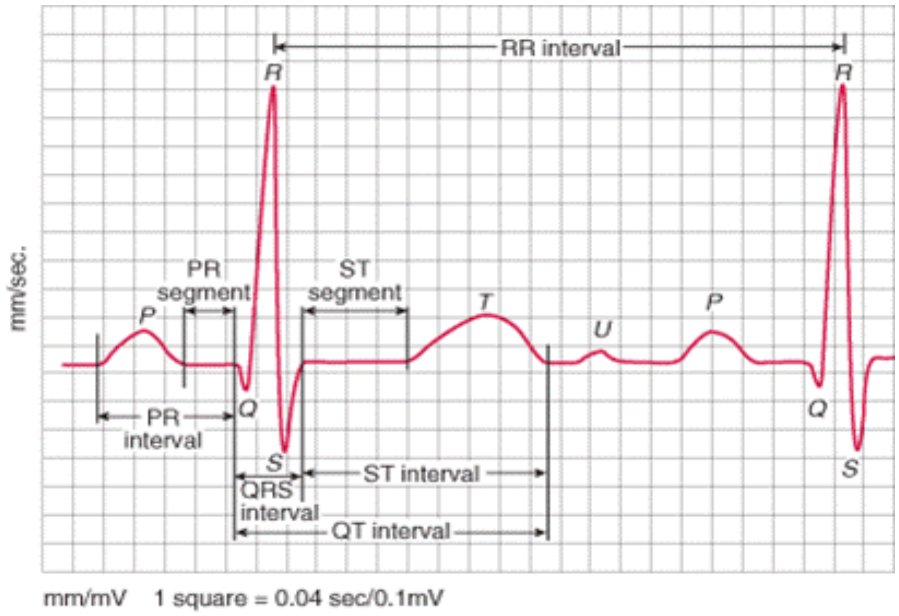

Figure 6. Representation of ECG from a normal sinus rhythm heart.
The graph represents the variations of potential as a function of time and consists of a sequence of waves (P, Q, R, S and T) and segments, which are repeated at each cardiac cycle (msdmanuals.com).

The P wave represents the electrical activation of the atria and it has a duration of about 100 ms. Activation of the sinus node does not produce measurable effects on the surface of the body due to its small size.

The segment PQ is the section following the wave P, has a duration of 100 ms and represents part of the repolarization of the atria. The repolarization is completed simultaneously with the invasion of the atrioventricular node and of the His bundle and gives rise to a wave defined as atrial T, not visible in the normal electrocardiographic traces because hidden by the QRS complex. The PQ interval constitutes the atrio-ventricular conduction time, which is normally between 120 ms and 180 ms, and it represents the passage of excitement from the atria to the ventricles.

The Q, R and S waves represent the ventricular invasion phase. The Q wave is the first negative deflection and corresponds to the activation of the interventricular septum; the R wave expresses the completion of the activation of the septum with the invasion of the apex of the heart; and the S wave represents the activation of the free walls of the ventricles and the base of the heart. The QRS complex, in its entirety, identifies the ventricular depolarization, and has a duration typically between 60 and 100 ms.

The section following the complex, the ST segment, appears to be of low potential, and represents the moment in which all the cardiac fibers are being depolarized.

Finally, the T wave is the expression of the completion of ventricular repolarization.

In some cases, the U wave is also visible, which could indicate the completion of the repolarization of Purkinje and/or myocardial fibers which have action potential duration longer than all others.

Arrhythmogenic syndromes

Cardiovascular diseases are the main cause of morbidity and mortality in western population (Huang et al., 2017). Sudden Cardiac Death (SCD) is one of the main causes of mortality in young individuals and is related to a series of predisposing genetic conditions, defined Inherited Arrhythmogenic Disease (IADs).

The hereditary arrhythmogenic diseases can be divided in two categories, depending on the type of predisposing mutation:

1) Cardiopathies, due to alterations of the cardiac structure;
2) Channelopathies, caused by mutations of ion channels and accessory protein.

Among the most widespread cardiopathies, there are the hypertrophic cardiomyopathies (HCM), whose origin is to be found in mutations, for example, of myosin and troponin ; the arrhythmogenic right ventricular dysplasia (ARVD) is due to mutations found in other protein such as plakophilins and desmosome and the dilatative cardiomyopathy (DCM), is also caused by genes mutations, not well characterized yet.

Channelopathies were first identified more than twenty years ago and, to date, more than 35 genes coding for different subunits or regulatory proteins involved in the arrhythmogenic syndromes are known (Abriel et al.,2015). The most widespread channelopathy is the long QT syndrome (LQTS), induced by mutations in several genes that increase depolarizing current, I_{Na} and I_{Ca} or that decrease repolarizing current (I_K). Another channelopathy associated with mutations in ion channels is Brugada syndrome, principally due to alterations found in sodium channels (Benito et al., 2008).

There are also other forms of congenital arrhythmias, including catecholaminergic polymorphic ventricular tachycardia (CPVT), short QT syndrome (SQTS) and mixed phenotypes.

Cardiac voltage-gated sodium channel ($Na_V1.5$)

Cardiac sodium channel (**Figure 7**) is a voltage-dependent channel constituted by an α subunit and several accessory β subunits with modulatory functions.

Nav1.5 is a glycosylated membrane protein with a molecular weight of about 220 kDa consisting of 2015 or 2016 amino acids (depending on the isoform).

The α subunit is composed by 4 homologous structural domains (DI-DIV), each of them consists of 6 transmembrane segments (S1-S6). Segments S5 and S6 are the pore-lining segments and the S4 helices serve as a voltage sensor. The three intracellular linkers as well as the N- and C-termini of the channel are cytoplasmic.

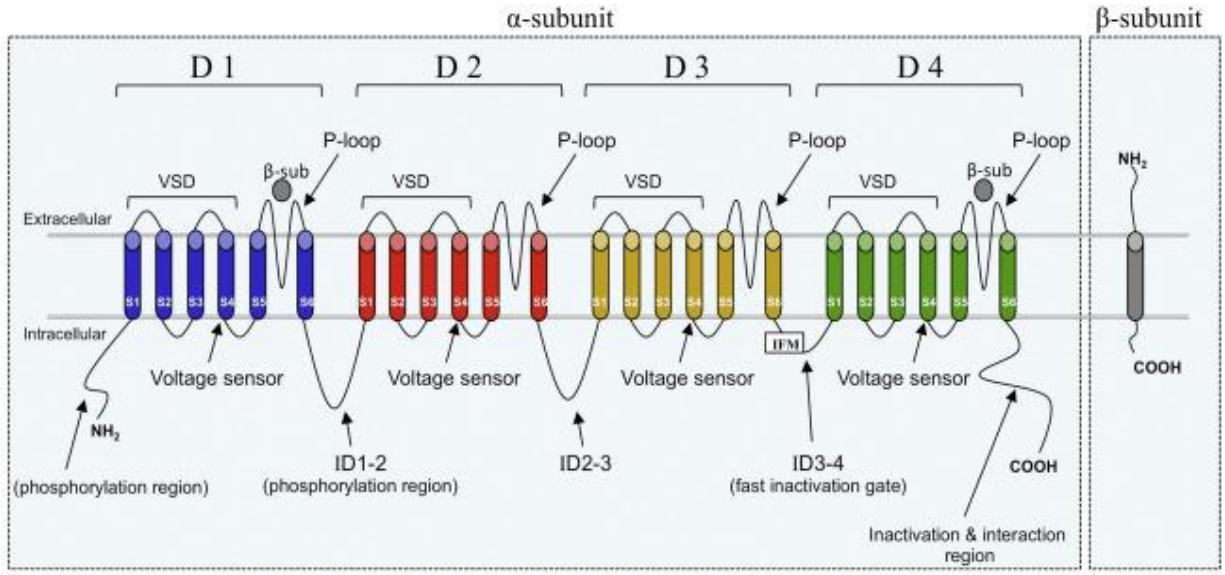

Figure 7. Cardiac voltage-gated sodium channel.
Schematic representation of Nav1.5; α subunit is shown, consisting of a single polypeptide chain in which it is possible to note the presence of 4 domains each formed by 6 transmembrane segments and the β subunit, also constituted by a single polypeptide chain (modified from sciencedirect.com).

SCN5A is the gene that encodes for cardiac α subunit and it is located on chromosome 3p21.

In the heart, the SCN5A transcript is abundant in the working myocardium and in the conduction tissue, while the expression in the sinoatrial and atrioventricular regions is relatively low. Four different splice variants (hH1, hH1a, hH1b, hH1c) have been identified in the human heart and they not only exhibit functional differences among themselves, but also different expression levels; the more express in human is hH1c, which it is found in the 45% of the population. (Makielsky et al., 2003).

hH1a, hH1b, and hH1c are characterized by the deletion of a glutamine (Q) in position 1077 compared to the hH1. There are more than 10 types of α subunit, differentially expressed in the heart and in other tissues, which have different electrophysiological properties.
β subunits are encoded by the SCN1B, SCN2B, SCN3B and SCN4B genes and consist of an extracellular N-terminal region that presents an immunoglobulin-like domain, a single transmembrane segment, and an intracellular C-terminal domain **(Figure 7**). β1 and β3 are associated non-covalently with the α subunit, while β2 and β4 form disulfide bonds. β subunits have important roles in modulation of channel function (such as voltage-dependence of activation and inactivation) and in its expression levels (increasing trafficking towards the membrane) (Veerman et al., 2015).
The sodium channel is part of a macromolecular complex that also includes sintrophin, ankyrin, caveolin, Nedd4-like ubiquitin ligase and calmodulin. These proteins are probably involved in regulation of channel activity, localization, biosynthesis and degradation (Ruan et al., 2009).

Pore structure and ion selectivity

Cardiac sodium channel pore is made up by:

1) a large outer vestibule, where binding sites for different toxins are present (for example tetrodotoxin);
2) a narrow selectivity filter;
3) a large central cavity filled with water;
4) an intracellular activation gate formed by the S6 segments (Catterall 2012).

The sodium channel is a selective channel that can select ions that pass through it. Its selectivity is based on two mechanisms: one dimensional and one electrostatic. Each channel allows the flow of ions smaller than a certain value; this turns out to be an intrinsic property of the channel itself. Furthermore, the ions, when crossing the pore, interact with the amino acid residues that delimit it, called coordination sites, which allow their stabilization. These interactions can be more or less strong, depending on the ion considered: if the ion is sufficiently stabilized, after a certain time of the order of nano seconds and pico seconds, its kinetic energy allows it to return to the solution or to pass to the second site of coordination, and so on until he can actually enter the cell. The presence of multiple binding sites creates one situation in which the more stable ion tends to have a repulsion on the less stable ion and repels it away. This ensures that permeability is therefore influenced not only by dimensional factors, but also by specific minimum energy

levels of the coordination points. This mode of passage is called multi-ion-single-file pore and ensures selectivity. About 20 amino acids are involved in the permeation and selectivity processes and they are located inside the P-loop that connects the segments S5 and S6.
The ion selectivity filter size of sodium channel allows the entry of a bound Na^+ ion to two planar water molecules. Negatively charged residues interact with the ion by removing part of the water molecules, but not all, and the Na^+ is conducted as a hydrated ion (Catterall 2012).

Activation

The cardiac sodium channel is a voltage-dependent channel, i.e. its opening depends on a membrane potential variation. Generally, the transmembrane electric potential is about -85 mV and, in this condition, the $Na_V1.5$ is in the closed state. When a depolarizing stimulus arrives and brings the potential to values more positive than -60/-70 mV, the channel opens. Around 20 mV, all channels are opened, reaching the maximum current density peak (**Figure 8**, red). The voltage-dependence of the activation of the sodium channel is due to the outward movement of three electrically charged residues present in the gate, in response to changes in the membrane electric field. The S4 transmembrane segments of all four domains indeed, contains a repeated motif (4 to 8 times) of positively charged amino acid residues (usually arginine) followed by two hydrophobic residues. The negative transmembrane electric field exerts a force on these positive charges causing their movement (Catterall 2000). In fact, according to the "sliding helix" theory, when the membrane depolarizes, the S4 segment can move outwards, causing a conformational change that opens the pore and allows the influx of Na^+ into the cell (Catterall, 1986)

Inactivation

Voltage-dependent ion channels, when subjected to a stimulus, remain open only for a short period of time, to then pass to a non-permeated state. The sodium channel, immediately after depolarization, become inactive in a few milliseconds and, therefore, the channel is unable to open again for a variable period of time. The inactivation curve (**Figure 8**, blue) represents the percentage of channels available at opening, depending on the membrane potential. The inactivation of Nav1.5 occurs with two different kinetics: fast inactivation, which occurs in a range of few tens of milliseconds, and slow inactivation, which takes place over a period of seconds.

Fast inactivation is mediated by the presence of an intracellular gate that binds the pore opening. In fact, the P-loop between the III and IV domains folds back into the channel structure like a lid. This segment has a triad consisting of an isoleucine, a phenylalanine, and a methionine (IFM motif) which is essential for fast inactivation and its folding is possible thanks to the presence of a couple of glycines (Catterall, 2000).

Slow inactivation, instead, involves conformational changes in the selectivity filter (Balser et al., 1996), where the S6 segment plays an important role in the transition to the inactivated state (Zhao et al., 2004). The complete slow inactivation is reached only after a period of time exceeding 60 s.

Between the fast and slow inactivation there is a possible condition, called intermediate inactivation, which can be reached during an action potential, but not by all channels. In fact, only a small fraction of channels is completely inactive, conducting a current called "sustained current" or "late current" (I_{NaL}).

Recovery from the inactivated state requires the repolarization of the membrane. During repolarization, the channels pass from the inactive state to the closed state, becoming again available to open in the next depolarization event. The recovery of the channels from the fast inactivation occurs within 10 ms, while the recovery from the intermediate and slow inactivation requires 50 ms and > 5s respectively.

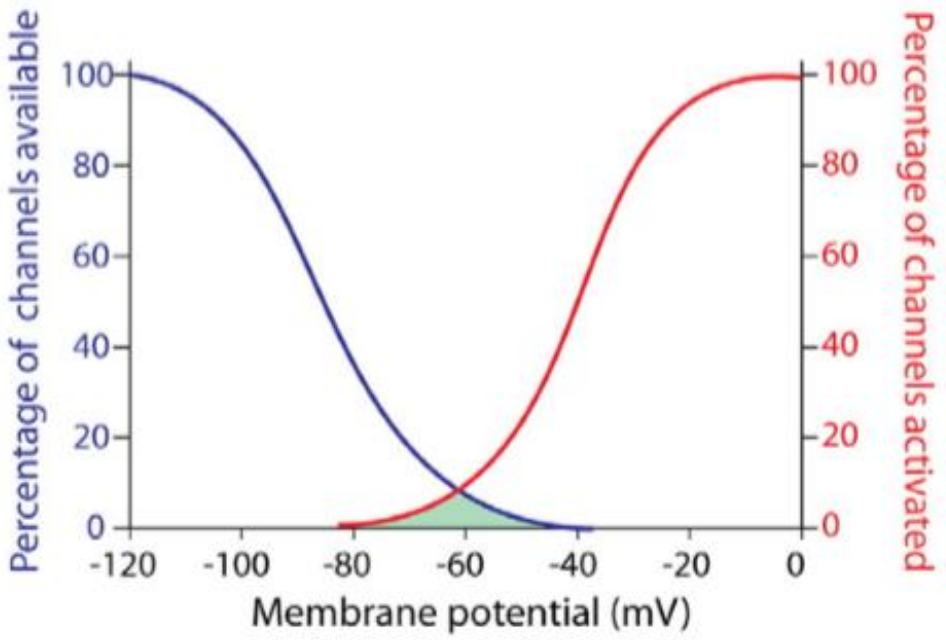

Figure 8. Activation/inactivation curves. Illustration of the Inactivation (blue) and activation (red) curves depending on membrane potential. The area subtended by the two curves determines the window current (green), (modified from Veerman et al., 2015).

Post-translational modifications

During the biosynthetic trafficking of the channel several post-translational modifications such as phosphorylation, arginine methylations, N-term acetylation and glycosylation may occur.
In its extracellular domain, the Nav1.5 protein presents some sites of N-glycosylation and the presence of glycosylation has an impact in the modulation of channel gating. Indeed, it has been seen that if Human Embryonic Kidney (HEK) cells are previously transfected with the hH1a isoform of Nav1.5 (ΔQ1077) with N-glycosylation inhibitors, a depolarizing shift is observed both in the activation and in the inactivation curve of the sodium channel. A similar situation was observed when treating rat ventricular myocytes (Rook et al., 2012).
It has also been seen that the rat Nav1.5 has about 13 KDa of carbohydrates and that the pattern of atrial and ventricular glycosylation is different. In fact, in atrial myocytes, proteins are more glycosylated than ventricular ones, reflecting the presence of chamber-specific maturation pathways (Marionneau & Abriel, 2015).
S-channel N-glycosylation begins in the endoplasmic reticulum. 40% of complex carbohydrates consist of sialic acid residues and are transferred to oligosaccharide acceptors in the trans-Golgi. In any case, the presence of these residues does not seem to be essential for the expression of the membrane sodium channel (Mercier et al., 2015).
Another post-translational modification that the sodium channel undergoes is phosphorylation, which, also in this case, modulates the kinetics of the channel. This type of modification is certainly the most documented about Nav1.5 and it is known that kinase pathways are implicated in the expression and/or functioning of the channel both in normal conditions and in case of pathology. Different proteins are involved in this pathway, including protein kinases A and C (PKA and PKC), Ca^{2+}/Calmodulin kinase II (CaMKII), phosphatidylinotol 3-kinase (PI3K), Fyn and AMPK (Marionneau & Abriel, 2015).
cAMP-dependent Protein Kinase (PKA) phosphorylates the Nav1.5 channel at different sites causing either an increase (Zhou et al., 2000) or a decrease in current densities (Sunami et al., 1991). The first two PKA phosphorylation sites were found in the DI-DII intracellular linker (rat: Serine 526 and Serine 529 corresponding to the orthologous human cardiac NaV1.5 isoform Serine 525 and Serine 528; Murphy et al., 1996).
Like regulation by PKA, the effects of Ca^{2+}/Calmodulin dependent protein Kinase II (CaMKII) on cardiac Na+ currents have been debated. A first report in HEK293 cells, by Deschênes and

collaborators suggested that CaMKII slows NaV1.5 channel inactivation and shifts the voltage dependence in the depolarizing direction (Deschenes et al., 2002).

A seminal work by Maier's group subsequently confirmed these findings (Wagner et al., 2006). Interestingly Ashpole et al. (2012) demonstrated that phosphorylation at sites S516, S571, and T594 (DI-DII intracellular linker) shifts the voltage-dependence of inactivation towards negative potentials, slows both the inactivation and the recovery from inactivation, and increases the late component of the INA (INa_L, Ashpole et al., 2012).

Protein Kinase C (PKC) is another enzyme implied in the phosphorylation of NaV1.5. Studies in cardiac ventricular myocytes indicated that activation of PKC reduces peak Na+ currents and shifts the steady-state current inactivation in the hyperpolarized direction, leading to a decreased probability of channel opening (Qu et al., 1994).

Cardiac NaV1.5 channels may also be substrates for the Adenosine Monophosphate-activated Protein Kinase (APMK), a regulatory mechanism that has been suggested to be responsible for the arrhythmogenic activity observed in Wolff-Parkinson-White patients that present with AMPK mutations and associated increased AMPK activity (Light et al., 2003). In this study, the authors showed, in a mammalian cell line, that a constitutively active AMPK mutant slows NaV1.5 channel inactivation with the appearance of a persistent Na+ current and shifts the voltage-dependence of NaV1.5 channel activation towards hyperpolarized potentials.

Recent evidence from the group of Richard Lin reported that the prolongation of action potential duration and QT interval, in the context of drug-induced long QT syndrome (Lu et al., 2012) and diabetes (Lu et al., 2013), is mediated, at least in part, by inhibition of Phosphatidylinositol 3-Kinase (PI3K) and the subsequent increase in late Na+ current. Accordingly, mouse hearts lacking the PI3K p110α catalytic subunit exhibit prolonged action potential and QT interval that are at least partly a result of an increased INa_L. The authors further demonstrated that the PI3K-dependent increase in INa_L in diabetic hearts is mediated by the inhibition of Protein Kinase B (PKB/Akt), a downstream effector of PI3K, and that inhibition of PKB/Akt by itself can also increase INa_L in non-diabetic cardiomyocytes. Together, these findings suggest that inhibition of the PI3K p110α subunit and downstream PKB/Akt mediates a common mechanism that adversely increases INa_L density.

Methylation is another form of modulation of NaV1.5. Proteomic analysis from a stable cell line that expresses NaV1.5 channels provided the first evidence that the Arginines R513, R526, and R680, located in the first intracellular linker loop of NaV1.5, are modified by methylation (Beltran-Alvarez et al., 2011). Each of the 3 Arginines was found to be monomethylated; R526 and R680 were also detected in a dimethylated state. The functional relevance of these findings

was further highlighted by the fact that R526H and R680H are mutations known to cause Brugada and long QT type 3 syndromes, respectively. A second study further demonstrated that the proteins Arginine methyl transferases (PRMT)-3 and -5 methylate NaV1.5 in vitro and increase NaV1.5 cell surface expression and Na+ current density (Beltran-Alvarez et al., 2013).

Functional characterization of a novel SCN5A mutation associated with Brugada syndrome.

INTRODUCTION

Brugada syndrome (BrS) is a cardiac channelopathy characterized by an abnormal electrical activity of the heart. BrS was firstly described by Italian authors in 1988 on the Giornale italiano di cardiologia (Nava et al., 1988). This pathology was then better characterized in 1992 by the Brugada brothers. The researchers carried out a study on 8 patients who had suffered from a single syncope event. This episode had been followed, in all cases, by a cardio-circulatory arrest, to which the patients had survived, thanks to cardiopulmonary resuscitation. None of them had any other problems before this event and did not present structural alterations in the heart. From the analysis of their electrocardiogram, common features emerged: blockade of the right bundle branch and elevation of the ST segment (Brugada & Brugada, 1992). To diagnose BrS, it is necessary to measure the patient's ECG, in the presence of drugs such as sodium channel blockers (class 1A and 1C antiarrhythmics) (Brugada et al., 2014).

Brugada syndrome is an autosomal dominant pathology and, most often, presents with an incomplete penetrance. Despite the high number of mutations found in patients associated with the disease, in only the 35% of the patients a genetic cause can be identified, whereas the remaining 65% turned out to be sporadic (Campuzano et al.,2010). BrS is a multifactorial disease that includes genetic, environmental and hormonal causes. Furthermore, compound mutations or common SNPs (single nucleotide polymorphism) may increase the risk of arrhythmias in these subjects (Brugada et al.,2014).

Most individuals do not present any symptoms, and this appears to be the main problem of this syndrome, in which the first manifestation often coincides with the death of the patient (Brugada et al., 2014). Sometimes symptoms can occur, such as tachycardia, atrial fibrillation, agonic breath, palpitations and chest pain. These problems tend to appear in association with an increase of vagal tone that occurs mainly during the night, in resting conditions or after a hearty meal. Furthermore, there is experimental evidence that body temperature can also act as a modulator of the pathology (Antzelevich, 2001). The early appearance of the symptoms generally occurs after the age of 40, however cases of patients suffering soon after birth are also

reported in the literature (Brugada et al., 2014). BrS is more common in South-East Asia, where a prevalence of 12:10,000 individuals has been estimated, compared to western countries where there is a prevalence of 1-5:10,000 (Berne & Brugada, 2012). Furthermore, men are more affected than women (8: 1), probably due to the hormonal influence and other factors implicated in pathophysiological mechanism. Previous studies have shown that testosterone levels appear to be higher in adult males suffering from the disease and, further studies in children, have not shown confirmed this prevalence since, children of both sexes, have low levels of testosterone (Polvina et al., 2017).

Since 1998, more than 350 mutations have been identified in different genes, including those that encode for cardiac sodium, potassium, and calcium channels and in several regulatory genes that encode for proteins involved in trafficking or in post-transduction regulation of these channels (**Table 1**, Watanabe & Minamino, 2016).

Gene	*Protein*	*Frequency*	*Functional abnormalities*
Na^+ channel dysfunctions			
SCN5A	α subunit Nav1.5	20-30%	INa^+
SCN10A	α subunit Nav1.8	Rare	INa^+
SCN1B	β subunit	Rare	INa^+
SCN2B	β subunit	Rare	INa^+
SCN3B	β subunit	Rare	INa^+
GPD1L	Regulatory protein	Rare	INa^+
MOG1	Regulatory protein	Rare	INa^+
SLMAP	Regulatory protein	Rare	INa^+
PKP2	Associated Protein	Rare	INa^+ ↓
Ca^{2+} channel dysfunctions			
CACNA1C	Cav1.2	1-3%	$ICa2^+$
CACNB2	β subunit	1-3%	$ICa2^+$
CACNA2D1	α-2delta subunit	Rare	$ICa2^+$ ↓
K^+ channel dysfunctions			
HCN4	IF channel	Rare	IK^+ ↑
KCNE3	β subunit	Rare	IK^+
KCNE5	Channel pore-forming α subunit	Rare	IK^+
KCND3	A-type K^+ channel	Rare	IK^+
ABCC9	Accessory protein	Rare	IK^+
KCNJ8	Kir6.1	Rare	IK^+
KCNH2	Kv11.1	Rare	IK^+
PKP2	Associated Protein	Rare	IK^+
Others			

Table 1. Gene mutations found in patients affected by Brugada syndrome.
(Frequency means the percentage of BrS patient associated with this mutation).

About 30% of the mutations concern the SCN5A gene, that encodes for cardiac voltage-gated sodium channel (Kapplinger et al., 2010): often are loss-of-function mutation and the common feature consists in the reduction of the current density. This decrease may be related both to intrinsic channel anomalous behaviors (such as altered voltage-dependence) and to defects in the trafficking of the α subunit. In literature, have been documented cases in which mutations, that cause retention of the channel in the cytoplasm, have been rescued by the use of drugs such as Mexiletine and Quinidine (Bezzina & Tan, 2002; Valdivia et al., 2002; Valdivia et al., 2004). As a general translational approach, the identification of the mechanism underlying a functional defect and its rescue represents a fundamental starting point for the development of a therapeutic strategies. In addition, *in vitro* studies have shown that the mutations can modify the kinetic properties of the sodium channel, such as slow recovery from inactivation, shift in the inactivation/activation curves towards more positive or negative potentials (Ruan et al., 2009).

Pathophysiological mechanism/s: a still unresolved issue!

The pathological mechanism/s of BrS is/are not clear yet, but two theories have been proposed:

1) "Repolarization theory";
2) "Depolarization theory".

The "Repolarization theory" proposes that the pathology is caused by a transmural dispersion of the repolarization in the right ventricle wall due to heterogeneity of the action potential between epicardium and endocardium, in particular in the outflow tract. Indeed, I_{to} (the transient outward potassium current that mediates phase 1 of the action potential), appears to be more prominent in the epicardium than in the endocardium and it is greater in the right ventricle than in the left. This could explain why the syndrome originates from the right side of the heart. Moreover, it could clarify the reason why the pathology is more frequent in males, since they have a higher Ito current density than females (Meregalli et al., 2005; Di Diego et al., 2002). Current difference between epicardium and endocardium causes an anomaly in the ECG that is called the *"J wave"*. Loss-of-function mutations of SCN5A channels decrease the inward current amplitude and causes a loss of the dome and abbreviation of the action potential. The loss of action potential dome in the epicardium but not in the endocardium is expected to create a voltage gradient during phase 2 and 3 of the action potentials that would be expected to manifest as a ST segment elevation. Loss of action potential dome at some sites but not others leads to the development of a marked dispersion of repolarization and steep voltage gradients within the

epicardium. Propagation of the action potential dome from sites at which it is maintained to sites which it is abolished causes a local reexcitation. This mechanism, termed phase 2 reentry, produces extra systolic beats capable of initiating one or more cycles of circus movement reentry. (Antzelevitch et al., 1999).

This hypothesis is not entirely accepted by the scientific community because some studies have shown that transmural repolarization is not present in some BrS patients (Tukkie et al., 2004), and results obtained using mouse models are controversial (Sendfeld et al., 2019).

The "Depolarization theory", argues that the pathology results from an increased fibrosis and a decreased number of gap junctions. This condition, combined with a reduction in sodium current, results in the slowing of the conduction of the right ventricle outflow tract, causing an elevation of the ST segment. Thus, differences in conduction velocity are created in different areas of the epicardium and can give rise to an epicardial re-entry excitation wave (Meregalli et al., 2005).

It is essential to remember that neither of the two theories can be considered the only mechanism capable of explaining the pathology and the two theories are not necessarily mutually exclusive (Brugada, 2016).

Currently, the use of a cardioverter defibrillator (ICD) is the only strategy to prevent SCD in BrS patients and moreover, it is necessary to avoid the administration of some drugs that can aggravate the ECG. Several pharmacological treatments are of common use, especially quinidine, isoproterenol, and phosphodiesterase III inhibitors, but further investigations are needed to clarify their benefits (Berne & Brugada, 2012). Experimental evidence shows that isoproterenol induces an increase in the L-type calcium current, while quinidine has an anticholinergic effect and blocks the I_{to}, resulting in a normalization of the ST segment elevation.

A further possible treatment of the pathology consists in the ablation of the right ventricle efflux tract area, onset site of ventricular fibrillation (Nademanee et al., 2011), indeed Pappone and colleagues firstly performed this novel surgical approach and found out that it can be considered a safe and potential way of preventing ventricular arrhythmia recurrences and sudden death in most patients with BrS (Pappone et al., 2017). However, there are still no evidences on long-term effects and benefits of RVOT ablations, for this reason we must remain cautious about the benefits of this treatment.

AIMS

Brugada syndrome, as mentioned in the introduction, is an autosomal dominant cardiac channelopathy with common electrocardiographic features such as blockade of the right bundle branch and elevation of the ST segment (Bugada et al., 1992). It is known that BrS has a genetic origin only in the 35% of the cases, while the 65% of the cases have a sporadic origin.

Our collaborators in Mazzoni Hospital (Ascoli Piceno, Italy) identified a novel SCN5A mutation S805L where the Serine 805 is substituted by a Leucine.

Therefore, during my Ph.D. period I focused on studying this mutation with electrophysiological and molecular tools in order clarify the biophysical properties of the mutation and to better understand the mechanisms that underlies the pathology.

RESULTS

The S805L mutation is characterized by the substitution of a Serine by a Leucine (a non-polar, instead of a polar aminoacidic). The mutation is located in the S3-S4 extracellular loop of the II domain and is the last residue before the beginning of the S4 voltage sensor (**Figure 9**). As I mentioned in the introduction, there are four different splice variants of Nav1.5 identified in the human heart (hH1, hH1a, hH1b, hH1c) and we decided to utilize the hH1c variant which is the more express in human heart.

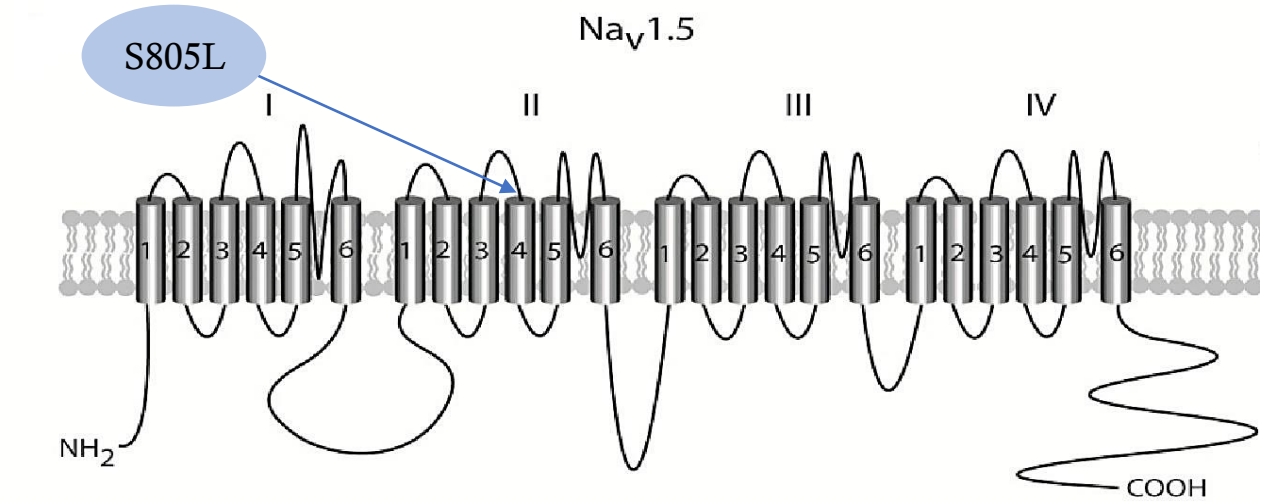

Figure 9. Localization of S805L mutation in Nav1.5 protein.

Using the SIFT software (Sorting Intolerant From Tolerant, a tool which predicts the functional outcome of a protein, based on the physic-chemical structure of its aminoacid composition) it emerged that the mutation could have a deleterious nature leading to pathological consequences since it has a score of 0.03 (scores ≤ 0.05 are predicted to be deleterious, while those ≥ 0.05 are predicted to be tolerated). Unfortunately, at the moment we do not have comprehensive information related to the clinical history of the patient. The cardiologist who is in charge of the proband is currently investigating this aspect. We know that both the son and the daughter of the proband carry the mutation and, provocative investigations have unleashed the BS phenotype in the son but not in the daughter. The prevalence of BS phenotype in males is a well-documented (Brugada et al., 2014) fact.

To assess the functional disruption of Nav1.5 activity caused by the mutation, we proceeded by evaluating the biophysical properties of the mutated channel.

We expressed the mutated channels in the Wild-Type (WT), Heterologous (Hetero), and Homologous (Homo) conditions in Human Embryonic Kidney cells (HEK 293), one of the principal heterologous system of expression used in electrophysiology.

We started considering the current density (**Figure 10**). Panel A shows representative traces and panel B the current-voltage (I/V) plot. Current traces were elicited by a train of depolarizing steps from -90 to +10 mV from a holding potential (hp) of -120 mV and in the figure are presented after normalization to cell capacitance. Data shown in the figure indicate that the S805L mutation significantly decreases the peak current density at all voltages investigated and this feature is voltage-independent (Panel C)

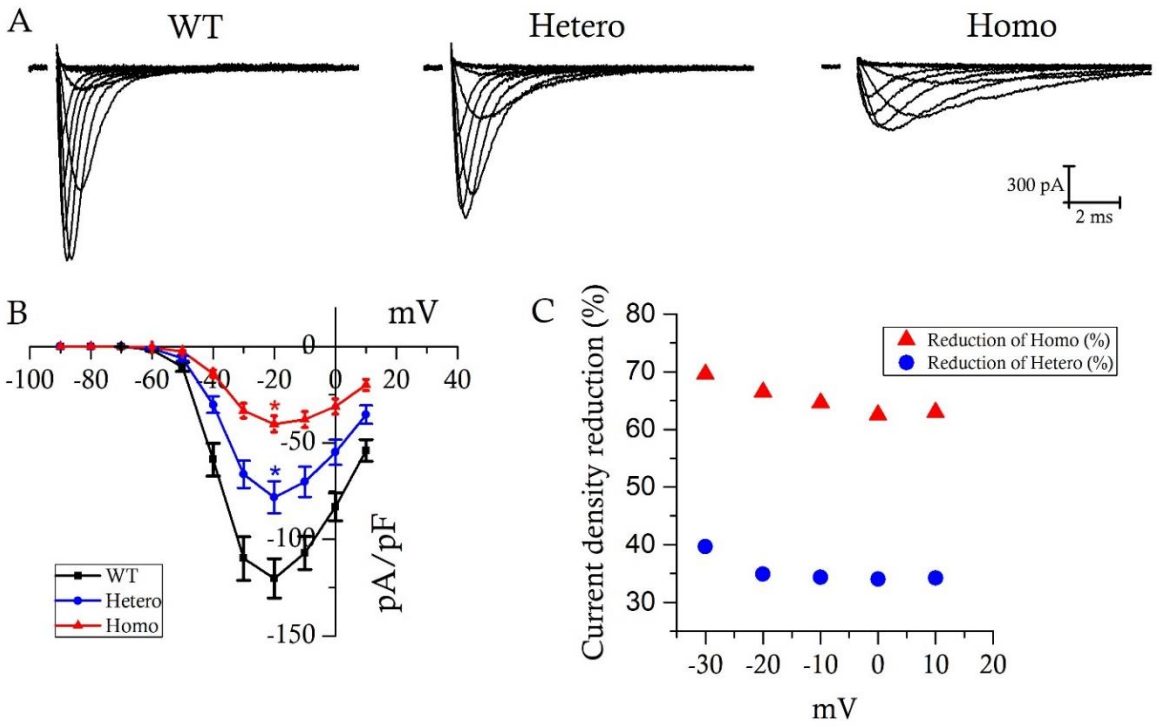

Figure 10. The S805L mutation reduces the INa peak current density.
(A) Representative current traces recorded in GFP-positive HEK cells transfected with WT, WT/S805L (Hetero), and S805L (Homo) hNav1.5 cDNA. (B) Mean I-V curves, normalized to cell capacitance. (C) Dot plot of percentage of reduction induced by the mutated conditions from -30 mV to +10 mV.

After these experiments, we moved on to consider the effects of the mutation on the kinetics aspects of the current (**Figure 11**). We first considered the inactivation profile by giving depolarizing steps from -140 mV to 0 mV of 1 s of duration. Cells were maintained at holding potential of -100 mV. Both Hetero and Homo conditions significantly positively shifted the

inactivation curves (Panel A) by 3.6 and 4.6 mV respectively (V½: -85.5±0.2 mV, n=55; -81.9±0.2 mV, n=25; -80.9±0.3 mV, n=22 for WT, Hetero and Homo, respectively, P<00.5). The activation curve was obtained by depolarizing voltages steps from -90 mV to +10 mV, and cells were maintained at a hp of -120 mV (Panel B). Results indicate that only the Homo condition significantly positively shifted the activation curve by 3 mV (V½, WT -33.0±0.4 mV, n=28; Hetero -32.3±0.1mV, n=27; Homo -30.0±0.3 mV, n=16).

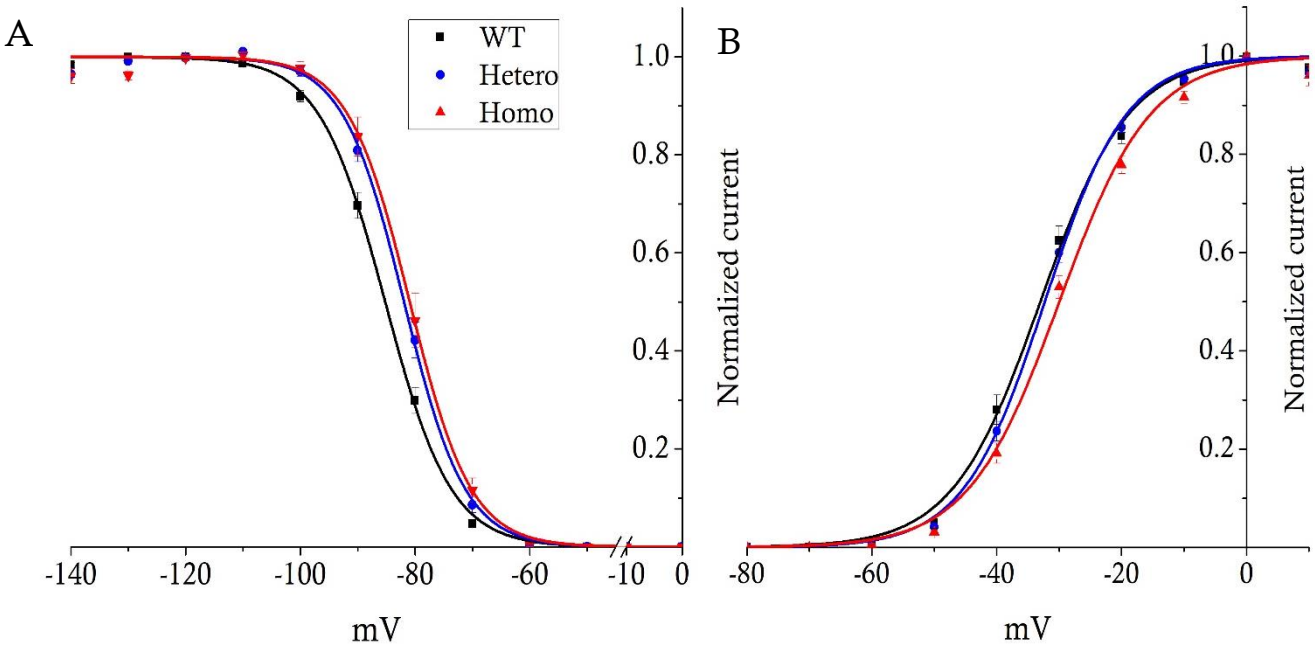

Figure 11. S805L mutation modifies the voltage-dependence of activation and inactivation.
(A) Mean inactivation curves obtained from WT, Hetero and Homo channels. Inactivation curves obtained in Hetero and Homo conditions are positively shift by 3.6 and 4.6 respectively. (B) Mean activation curves of WT, Hetero and Homo channels. The activation curve obtained in Homo condition is positively shifted by 3 mV.

Following these experiments, we next considered the recovery from inactivation (**Figure 12**), a parameter that is strictly connected to the refractory period of the channels. The recovery from inactivation was obtained by a double pulse protocol. Cells were depolarized to 0 mV for 50 ms from a hp of -120 mV, then returned to the holding potential with an interval from 0.4 to 13.2 s and a second step of 50 ms to 0 mV was then delivered. Panels A, B, and C show representative traces of WT, Hetero, and Homo respectively. The first trace of each panel depicts the first test step, while the others represent the following step after three different recovery times (1 ms, 5 ms, and 13 ms). In panel D mean±sem data of normalized current amplitude ratios (I_{2step}/I_{1step}) obtained in the three conditions are presented. Data were fitted by a mono-exponential function and the time constants of the fitting lines are: WT 2.81±0.1 ms, n=16, Hetero 2.48±0.1 ms, n=16 and Homo 3.0±0.1 ms, n=10 (not significantly different; Anova One-Way).

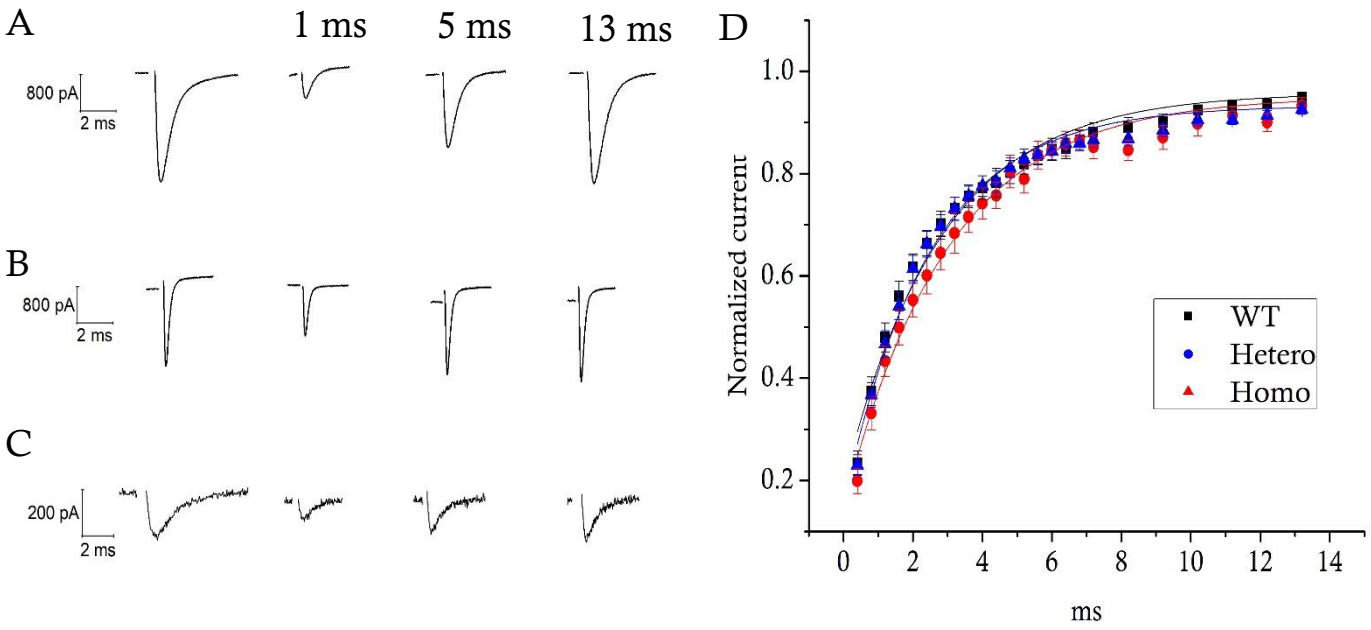

Figure 12. The S805L mutation does not alter the recovery from inactivation. (A, B, and C) show representative traces of the recovery from inactivation of WT, Hetero, and Homo respectively. (D) Mono-exponential fitting was chosen as a simple approach to compare the time course of the three conditions.

Then I considered the kinetics of inactivation of the sodium current, since any change in these parameters may also be relevant. The inactivating part of the current was fit with a mono-exponential function and time constants of current decay are shown in **Figure 13**. Clearly, the presence of the mutation in the Homo condition cause a slowing of the rate of inactivation; data on the Hetero condition are less clearly interpretable (Anova One-Way).

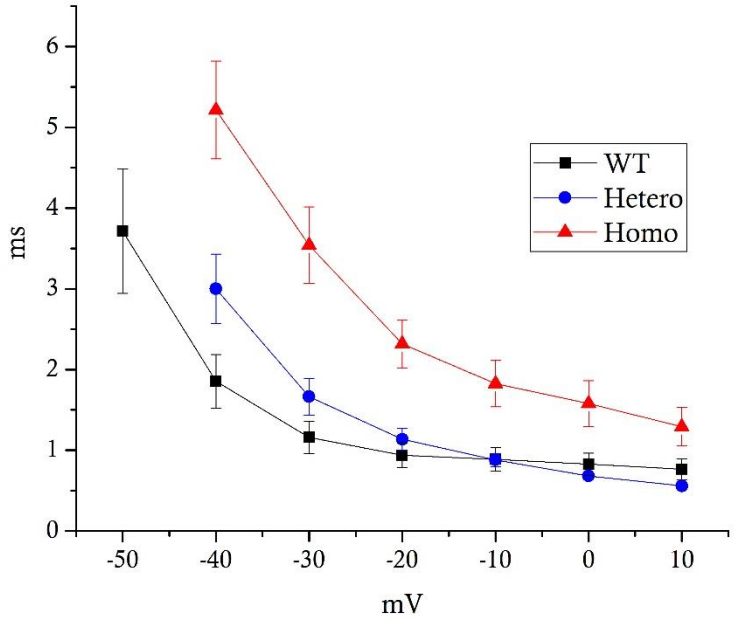

Figure 13. The Hetero S805L does not impact the time constant of inactivation of the channels. Time constants of inactivation obtained by fitting the sodium current decay with a mono-exponential function (WT n=8; Hetero n=8; Homo n=8).

We also decided to evaluate the effect of our mutation on the long-lasting component, named "late" (INa_L), of the sodium current (**Figure 14**). To this aim we elicited the current by stepping to -20 mV for 250 ms (holding potential, -120 mV) in the presence and absence of TTX (30 μM), and we focused our analysis on the last 50 ms of the current, that is when the current is at the steady state. In this case we did not find any significantly difference in the three conditions (WT -0.66±0.19 pA/pF, n=14; Hetero -0.41±0.1 pA/pF, n=12; Homo -0.36±0.1 pA/pF, n=11).

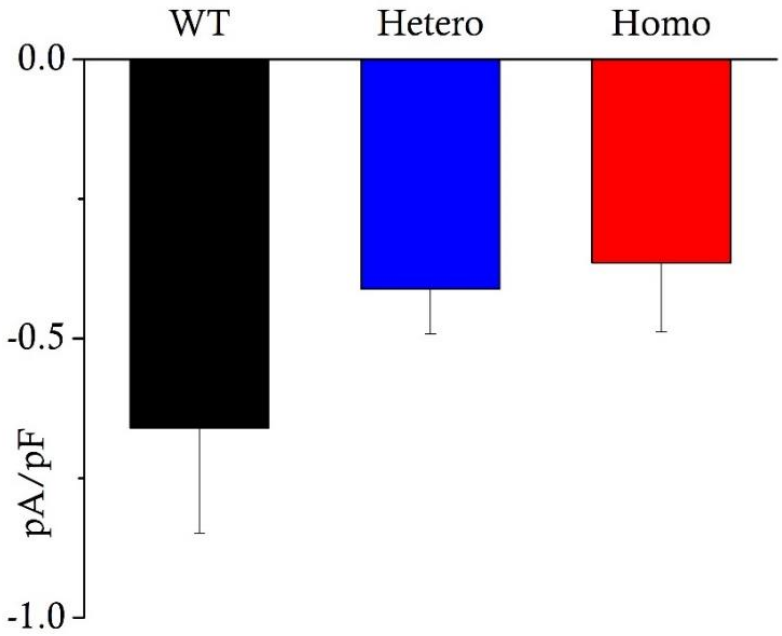

Figure 14. The S805L does not impact on late sodium current.
Bar graphs show the mean current density calculated between 170 and 220 ms of the protocol.

We then decided to assess the behavior of the mutation at three holding potentials (-120 mV, -100 mV, and -80 mV panels A, B, and C of **Figure 15**), in order to understand whether the physiological holding potential may have an impact on the effect of the mutation. This is particularly relevant since the physiological resting potentials of cardiac cells is in the order of -80/-90 mV. In the Hetero channels the effect of the mutation (**Figure 15** D) on the current density decreases at progressively more depolarized holding potential. (Mean peak current densities are presented in **Table 2**).

	pA/pF at -120 mV	pA/pF at -100 mV	pA/pF at -80 mV
WT	-120.2±10.2 n=28	-96.1±6.2 n=80	-45.4±5.5 n=21
Hetero	-78.2±8.3 n=27	-74.5±7.3 n=33	-37.5±3.3 n=33
Homo	-40.3±4.2 n=16	-29.1±2.1 n=49	-21.5±2.4 n=14

Table 2. Peak current density at holding potential of -120, -100, and -80 mV.

Based on these results, we can conclude that the mutation does not influence the size of the Hetero current at physiological holding potential of -80 mV, but it starts to exert a robust action when the cell hyperpolarizes.

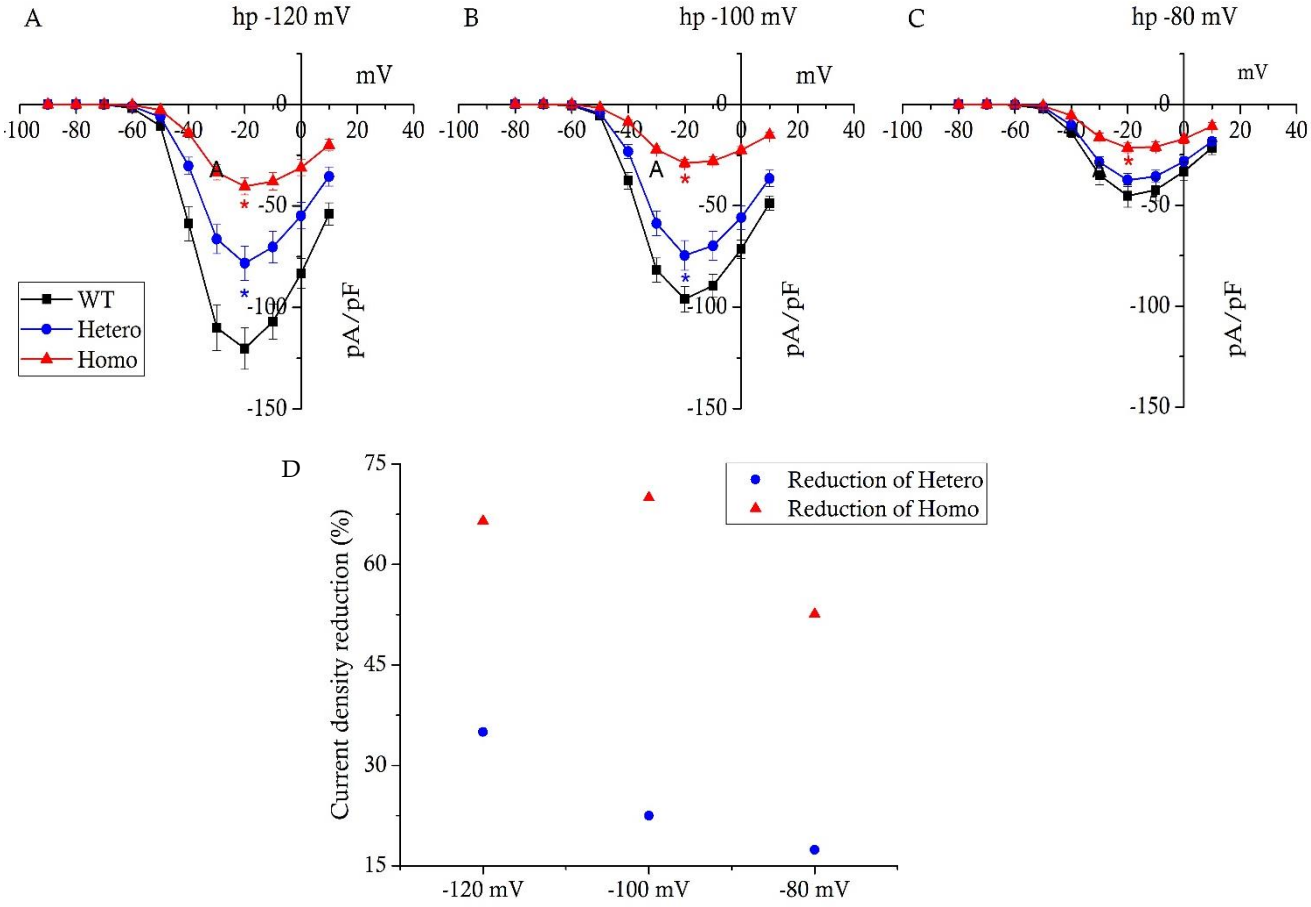

FIgure 15 The effect of the heterozygous S805L mutation on the current density depends on the holding potential.
(A, B, C) Mean I-V curves obtained for WT, Hetero, and Homo at holding potential of -120 mV, -100 mV, and -80 mV respectively, * P<0.05 at -20 mV. (D) Current density reduction (%) of Hetero and Homo compared to WT.

Since at physiological resting potential (around -80 mV) the mutation does not seem to exert a significant action, while at more hyperpolarized potentials the effect is robust, we were interested in assessing whether the cells of the right ventricle, which is the site of origin of BrS, may present with variation of the holding potential in different physiological conditions. During patch-clamp experiments we verified that the resting potential of guinea pig right ventricular cells was significantly influenced by the rate of stimulation. In particular the higher the rate of stimulation, the more positive the resting potential; sample recordings are shown in panel A,B,V, while the box-plot distribution of actual resting potentials are shown in **Figure 16 C.** Mean±Sem values are: 4 Hz -80.7±06 mV, n=17; 2.5 Hz -81.8±0.6 mV, n=18; 1Hz -82.9±0.6 mV, n=19.

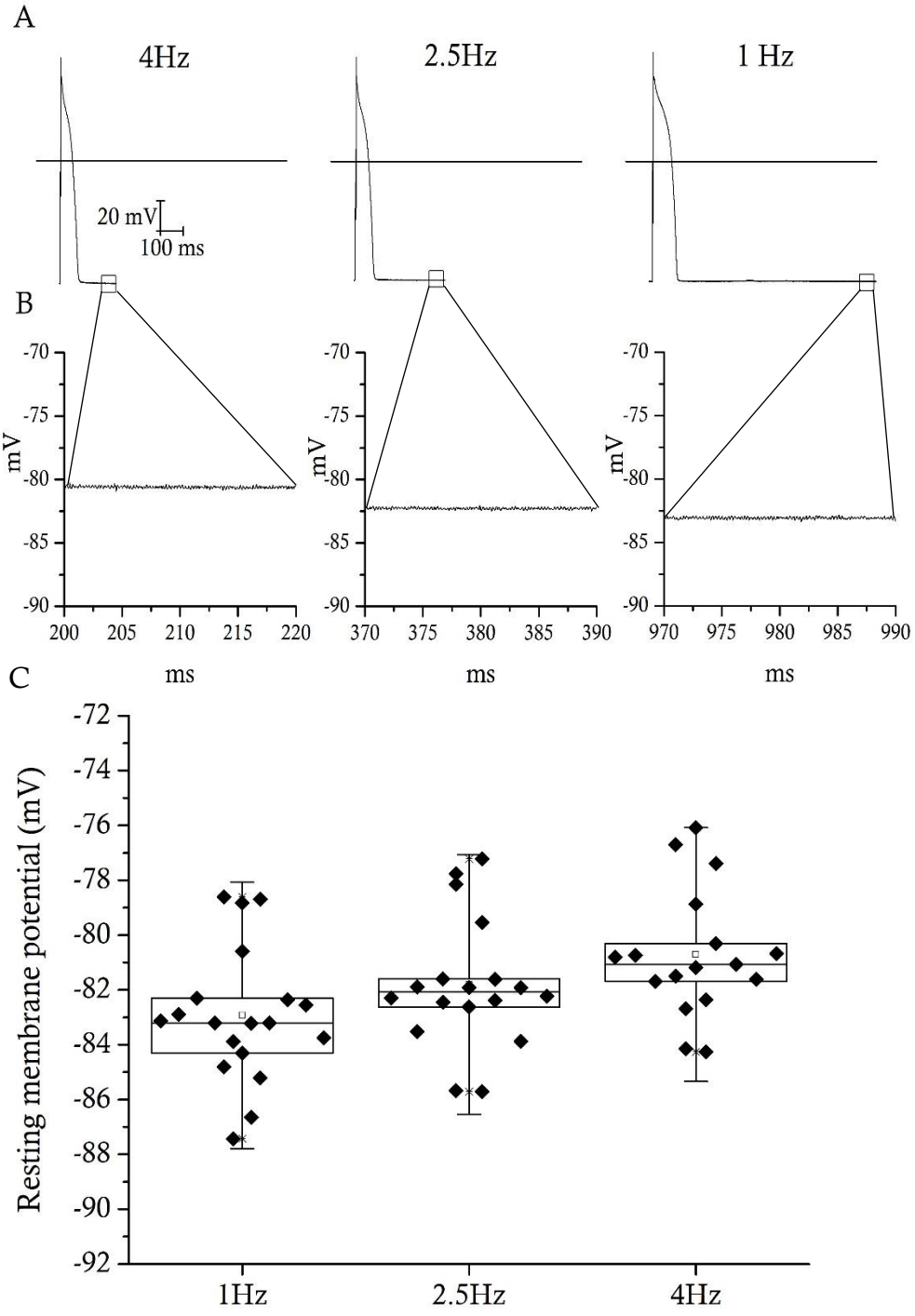

Figure 16. Effect of different stimulation frequencies on resting membrane potential.
(A) Representative traces action potentials stimulated at 4 Hz, 2.5 Hz, 1 Hz respectively. (black lines are positioned at 0 mV. (B)Zoom of panel A that shows an example of resting membrane potentials decrease got through different stimulation frequencies. (C) Box plot of mean resting membrane potentials measured.

We then moved on to assess the protein levels by Western Blot experiments. WB of total protein extract is shown in **Figure 17.** Blotted proteins were probed with an anti-hNav1.5; an anti-actin antibody was used as internal control for the normalization of $Na_V1.5$ signals in the quantitative analysis. Panel A shows the specificity of the antibody since the bands relative to $Na_V1.5$ are not present in the non-transfected condition. In the transfected lanes (WT and Homo/S805L) three

major bands are instead visible and represent the fully glycosylated, partially glycosylated, and non-glycosylated conditions. Panel B shows an example of WB on which we performed the densitometrical analysis. Data shown in the panel C represent the total signal generated by the three bands: a significantly difference in the expression of $Na_V1.5$ between Homo and WT is present. The quantitative analysis confirmed of the fully-glycosylated form also confirmed a higher level of expression for the WT channel (panel D). We also found that the WT and Homo conditions display a significantly difference in the ratio of the fully glycosylated versus partially glycosylated $Na_V1.5$ proteins (panel E), suggesting that the mutation causes a lower translocation of the mature protein into the membrane.

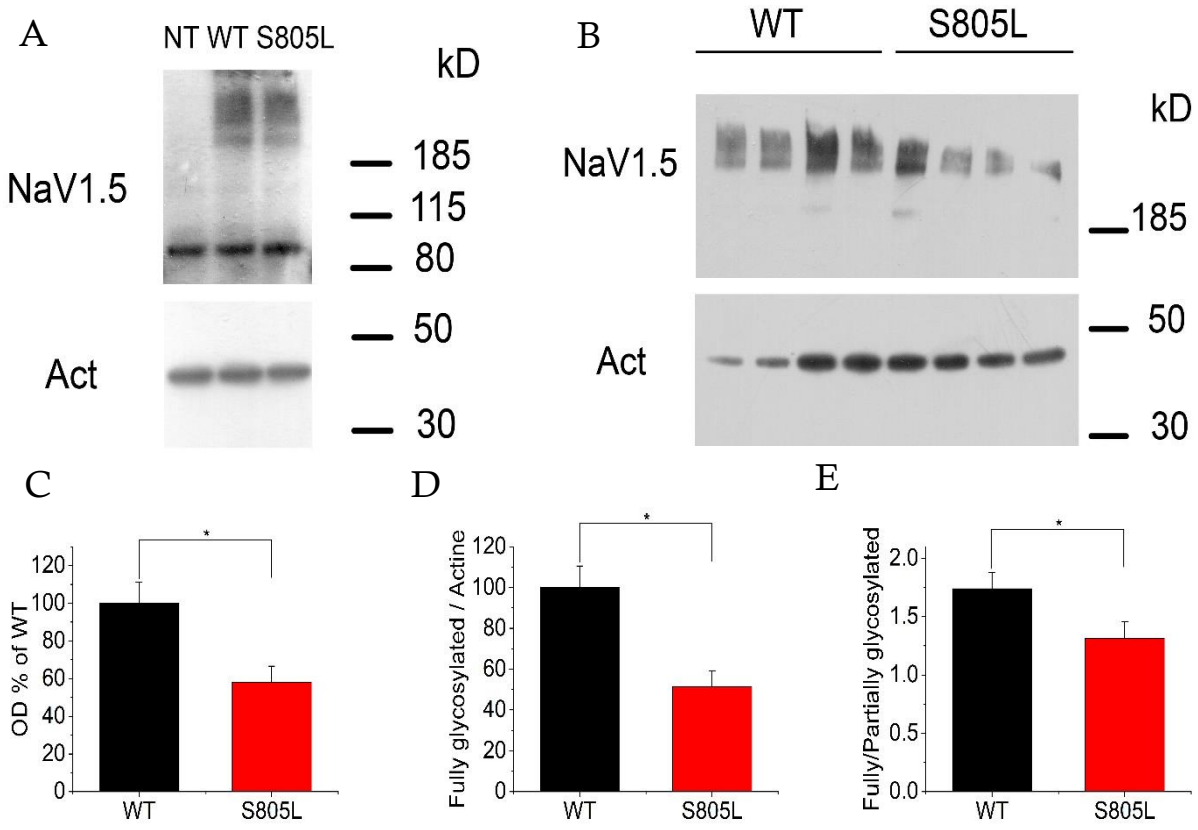

Figure 17. Western blot of total protein extracts from HEK-293 cells transfected with WT and S805L Nav1.5.(A) Western blot of total membrane extracts from not-transfected HEK cells (NT) and WT $Na_V1.5$ or S805L $Na_V1.5$-tranfected cells (B) A representative WB of four independent protein extracts from WT Nav1.5-trasfected HEK cells and four independent S805L $Na_V1.5$-trasfected cells. The same amount of proteins was loaded in all lanes; actine (Act) was used as housekeeping gene for the normalization of the Nav signals. (C) Bar graphs of total glycosylated protein amount; Significant difference was found in the expression levels of WT and mutated Nav1.5 proteins (WT=100.0%±11.1; S805L=58.1%±8.4; n=12, t=0.001). Values are expressed as percentage of the WT. (D) Bar graphs indicated the Fully glycosylated band normalized to the Actine of WT and S805L proteins (WT: 100±10.6; S805L: 51.5±7.7; n=12, t=0.0002). (E) Bar graphs indicated the ratio between fully glycosylated and partially glycosylated of WT and mutated $Na_V1.5$ proteins (WT: 1.74±0.14; S805L 1.32±0.14; n=12, t=0.015).

DISCUSSION

Brugada syndrome is an autosomal dominant cardiac channelopathy that was described for the first time by Italian authors in the late eighties of the last century. The ECG of these patients has common features, such as blockade of right bundle branch and elevation of ST segment (Brugada & Brugada, 1992). The majority of individuals who suffer from BrS remains asymptomatic and, in most of the cases, the first clinical manifestation of the pathology coincides with the death of the patient (Brugada et al., 2014).

More than 350 mutations in different genes have been studied in the last decades and here I presented a novel mutation identified in a male patient who suffer from Brs. Our collaborators at Mazzoni Hospital (Ascoli Piceno) found a novel heterozygous single-nucleotide mutation S805L, which is characterized by the substitution of a polar residue (Serine) by a non-polar one (Leucine) in position 805, that corresponds to the last residue before the S4 voltage sensor of the II domain of the protein (**Figure 9**).

In order to unravel the peculiarities of the mutation, we proceeded with a software analysis using the SIFT algorithm and the result was compatible with the clinical phenotype of the patient, indeed the software yielded a score of 0.03 predicting a deleterious nature of the mutation. As usually happens in this type of works, we first wanted to evaluate the biophysical features of the mutation and we analyzed the effect of S805L on current density (**Figure 10**). The loss-of-function nature of the mutation was immediately clear because it reduced current density by 66.5% in the Homo condition and by 35% in Hetero one.

We then verified the different kinetic parameters, not merely limiting ourselves to describing macroscopically the problem, but going into the details of the biophysics of the mutation. Among these parameters, we first analyzed the voltage-dependence of activation and inactivation of the channels (**Figure 11**). Both Homo and Hetero shifted toward positive potentials the inactivation curve by about 4.6 mV and 3.6 mV, respectively. Also, the activation curve of Homo is shifted toward more depolarize potentials by 3 mV, while in the Hetero condition there were no changes in the voltage-dependence of activation. The positive shift of inactivation curve should by itself increase the Hetero and Homo currents compared to WT, indeed at the same voltages there are more channels available to open, and this phenomenon should contrast the robust current density reduction observed before and try to rescue the phenotype. On the basis of these results we can add that, in our case, any modulation that shifts the inactivation curve to the left is

proarrhythmic, while if it shifts to the right it is protective (see post-translational modifications paragraph in the introduction; further comments later on). We have researched in the literature whether the mutation at position 805 studied by us was or was not the site of post-translational modifications, such as phosphorylations, methylations, etc., but we did not find any experimental evidences.

We went on to evaluate the recovery from inactivation (**Figure 12**), and the time constants of inactivation (**Figure 13**) of the channels. We found no changes among the three different conditions, albeit Homo time constant of inactivation was slower compared to the other.

We have also taken into consideration the "late" sodium current, which is the long-lasting component of this ion flux. INa_L is much smaller than the transient component of the sodium current in normal ventricular myocytes, but it may be enhanced by several fold under pathological conditions (Berecki et al., 2006), such as LQT3 syndrome that is characterized by a prolongation of action potential duration. Although Brugada syndrome is not characterized by an increase of the ventricular action potential duration, we wanted to measure the INa_L to effectively exclude its involvement in the pathophysiological mechanism. Our data, shown in **Figure 14** confirmed these evidences; indeed, we did not find any difference among the three conditions.

Under physiological conditions, ventricular cells have resting potentials of about -80 mV, however our results (see figure 10) were collected at -120 mV of holding; for this reason, we planned additional experiments to test for possible difference in the behavior of the mutation when its effect are tested at different holding potentials. We decided to study the effects of the mutation using two additional holding potentials (-100 mV and -80 mV) in order to better mimic the physiological condition of the channel in the heart environment (**Figure 15**). When the Hetero and WT I/V curves are compared, it can be noticed that their difference is small or absent at the holding potential of -80 mV, but they display a significant different profile at holding level of -100 mV and -120 mV. Based on these results we reasoned that any condition that contributes to the hyperpolarization of the holding potential should unleash the pathological phenotype of the mutations. In other words, at potentials of -80 mV mutant and WT channels behave similarly and no BrS event can occur, but when the potential hyperpolarizes mutant channels can trigger the appearance of BrS. Interestingly, it is a well-known evidence that BrS, often occurs in the presence of vagal tone hyper activation. We therefore tested whether the resting potential could be affected by the bradycardic action induced by vagal activity. For this reason, we performed current-clamp experiments stimulating guinea pig ventricular cells using different stimulation

frequencies. As shown in **Figure 16** the cell membrane potential decreased from -80.7±06 mV at 4 Hz to -82.9±0.6 mV at 1 Hz.

Along with the electrophysiological experiments, we also performed Western Blot analysis on total protein extract in order to verify if there were any problems in terms of transcription, translation, and protein trafficking of the channels (**Figure 17**). The Nav 1.5 expression level was reduced by about the 50% in the mutated condition compared to WT; furthermore, the active channels (fully-glycosylated form) is also less expressed in our mutation. We observed other modifications that alters Nav 1.5 trafficking: this is due to the reduction of ratio between fully glycosylated versus partially glycosylated forms of the channels.

Putting together all the electrophysiological and molecular data we can conclude that S805L causes a strong reduction of current density combined with a robust reduction of protein expression levels and this is in agreement with other evidences that are still present in the literature.

The novelty of our work is to be found in the anomalous behavior of the mutation at physiological potentials. Is the reduction of ventricular cardiomyocytes resting potential enough to explain the pathophysiological mechanism? We do not have the correct answer, but the most appropriate probably is, no. Certainly, other factors could participate to give rise to the pathology, for example, we have to consider the circadian rhythm of ion channels: it's well known that the expression of ion channels, such as other protein, follows the circadian rhythm. Black and colleagues (Black et al., 2018) nicely showed that the mouse sinoatrial circadian clock controls HCN4 mRNA, HCN4 protein, and the corresponding I_f in a circadian manner. Indeed, the I_f is higher in the awake period, appropriately explaining the higher heart rate. Not only HCN4 is regulated in a circadian manner, but also other channels, such as Nav 1.5 (Schroder et al., 2013), TASK-1, Kv 1.5, Kv 4.2 (Black et al., 2018). Since BrS mainly occurs at night, we can speculate that during the asleep phase the expression level of Nav 1.5 is smaller and therefore, a current density reduction is possible to be observed. Moreover, it is well known that the cell membrane resting potential is regulated by serum potassium concentration: high potassium concentration means that the resting membrane potential become more positive and vice versa. This concentration fluctuates from 3.5 mEq/l to 5 mEq/l in physiological conditions (Heras & Fernandez-Reyes, 2017), and in a circadian manner (Schmidt et al., 2014): the lowest concentration was measured at 9 p.m., while the highest at 1 p.m. For the same reason that BrS occurs at night and the lowest potassium concentration is observed at 9 p.m., we can speculate that at low serum potassium concentration the cell membrane potential decrease, and together

with the phenomenon described before (a lower heart rate corresponds to a more negative resting potential) we could explain what happens in S805L mutation.

About future perspectives we intend to verify the resting potential of the cells in conditions of hypo / hyperkalemia in order to support our speculations. Furthermore, we intend to insert all our results in a mathematical model of ventricular action potential to compare the different conditions.

Biophysical study of SCN5A compound mutations found in a child with sinus node dysfunction, atrial flutter, and drug induced long-QT syndrome.

INTRODUCTION

This second project in which I have been involved started with a case report of a two-year-old patient that was taken to the Azienda Ospedaliera Papa Giovanni XXIII (Bergamo) with a severe, asymptomatic bradycardia and recurrent atrial flutter episodes (DeFilippo et al., 2015).
Before presenting this case, I will briefly introduce what sinus node dysfunction (SND) and atrial flutter are. SND is generally used to identify various pathological conditions related to inability of sinoatrial node (SAN) to generate heart rate in an appropriate mode for the physiological needs.
Various cardiac disorders such as inappropriate sinus bradycardia and tachycardia, sinus arrest, sinus-exit block alternating periods of bradycardia and tachycardia, and chronotropic incompetence are recognized as manifestations of sinus dysfunction (Benson et al., 2003). The etiology of SND can be intrinsic, extrinsic or often a mixture of the two. One retrospective study of 277 patients presenting to the emergency department with compromising bradycardia showed that 51 % of cases were attributable to a treatable extrinsic cause such as an adverse drug reaction, electrolyte imbalance or acute myocardial infarction. The other 49 % were assumed to be intrinsic or idiopathic (Sodeck et al., 2007).
The pathophysiology of idiopathic SND is still not well understood (Choudhury et al., 2014). Historically it is attributed to fibrosis and cell senescence and this is often still quoted today (Thery et al., 1977; Evans & Shaw, 1977). However, contemporary evidence suggests that electrical remodelling of molecular pacemaking mechanisms such as membrane ion channels and intracellular Ca2+ cycling are important factors in SND (Morris & Kalman, 2014).
In cardiac SAN cells, the presence of Nav1.5 channels has long been debated. There are now evidences that in most of animal model investigated, Nav1.5 channels are absent or scarce in the center of the SAN, while they are widely expressed in the periphery where the functionally contribute to impulse conduction (Honjo et al., 1996; Baruscotti et al., 1996; Remme et al., 2009). Despite the absence of Nav 1.5 channels in the center of the SAN, there are lots of

evidences that many SCN5A mutations are associated with inherited SND, such as bradycardia and sinus exit block (Milanesi et al., 2014).

Atrial flutter (AFL) is one of the most common supraventricular arrhythmias (Granada et al., 2000) and is characterized by an atrial rate of about 300 beats/min and faster than normal ventricular rate that can be fixed or variable associated with palpitations, fatigue, syncope, and embolic phenomenon (Bun et al., 2015). AFL afflicts ~0.19 million people in the United States in 2005 and its prevalence is expected to increase to 0.44 million by 2050 because of the aging of the population (Naccarelli et al., 2009). Animal and human studies have shown that AFL is usually preceded by a transitional period of atrial fibrillation (AF), (Waldo et al 2008). Because of the dependence of flutter on fibrillation, the two arrhythmias commonly coexist clinically, with documented AF up to 75 % of AFL patients. (Mittal et al., 2013). Atrial flutter is common in patients with underlying diseases such as chronic obstructive pulmonary disease, pulmonary hypertension, and heart failure. Isolated atrial flutter in the absence of abnormal heart anatomy is rare and is instead usually present when atrial size abnormalities have developed. Atrial flutter is more frequent in males than in females. Aging is a significant risk factor and patients presenting with atrial fibrillation, systemic hypertension, diabetes mellitus, and history of alcohol abuse (Halligan et al., 2004) are more prone to develop AFL.

AFL is a macro-reentrant tachycardia and, depending on the site of origin, can be typical or atypical (Bun et al., 2015). The Todaro tendon, crista terminalis, the inferior vena cava, the tricuspid valve annulus, and the coronary sinus delineate the circuit of the typical AFL. These structures are essential to provide the pathway length for the flutter system. The mechanism of arrhythmia is a macro-reentry activation of the right atrium from the interatrial septum and along the crista terminalis with passive activation of the left atrium via the coronary sinus muscular connection (Klein et al., 1986; Kalman et al., 1997).

The atypical AFL is independent of the CTI, and the origin of the arrhythmia can be in the right atrium or the left atrium. Electrophysiologic studies and intracardiac mapping are the only means to determine the exact mechanism or area generating the atrial flutter. Different from typical AFL, the presence of atypical AFL is related to structural heart diseases as prior cardiac surgery or ablation procedures (Tai & Chen 2009). When the AFL is determined to come from the right atrium but not associated with the CTI system, the circuit can be in the superior vena cava and part of the terminal crest. When prior surgery or intervention occurred, the presence of scar can often become arrhythmogenic, and the center of the circuit and the onset of the arrhythmia mostly occur after several years of the procedure, likely secondary to remodeling (Cosio 2017). In patients without prior cardiac intervention, the AFL circuit can be low voltage

areas like the lateral right atrium, this might be secondary to fibrosis due to chronic atrial high pressures, or cardiomyopathy that can produce fibrosis of the myocardium and creating low voltage areas that allow atrial flutter to occur (Kall et al 2000). Without focusing on the clinical counterpart, I will now move on with my experiments.

AIMS

This is a new project that started in collaboration with our clinical colleagues in Azienda Ospedaliera Papa Giovanni XXIII (Bergamo). They identified compound mutations in the SCN5A gene for paternal K1578N and maternal G1866fs. Family history was unremarkable and both parents were asymptomatic and with normal ECG.

After the clinical characterization, made by the medical doctors at the hospital, I started studying and elucidating the molecular mechanism that originate this peculiar multifactorial pathology.

RESULTS

A two-year old patient was hospitalized because a severe but asymptomatic bradycardia and recurrent atrial flutter episodes. After several treatments, MDs decided to implant a pacemaker in order to prevent other possible symptoms: this was a tricky case of pediatric overlap syndrome. Genetic analysis revealed compound mutations in the SCN5A gene: the father (p) was a carrier of heterozygous K1578N and the mother (m) of heterozygous G1866fs. The first one is a missense mutation that is characterized by a substitution of a Lysine by Asparagine in position 1578, localized in the transmembrane segment S2 of the fourth domain, while the second one is a frameshift mutation resulting in a shortened protein (deleting the terminal 150 amminoacids) and it is located in the C-terminal of the protein (**Figure 18**). Considering the age of the patient, we decided to choose the neonatal isoform of cardiac sodium channel, although there are is clear evidence indicating at which age after birth there is the switch of isoforms.

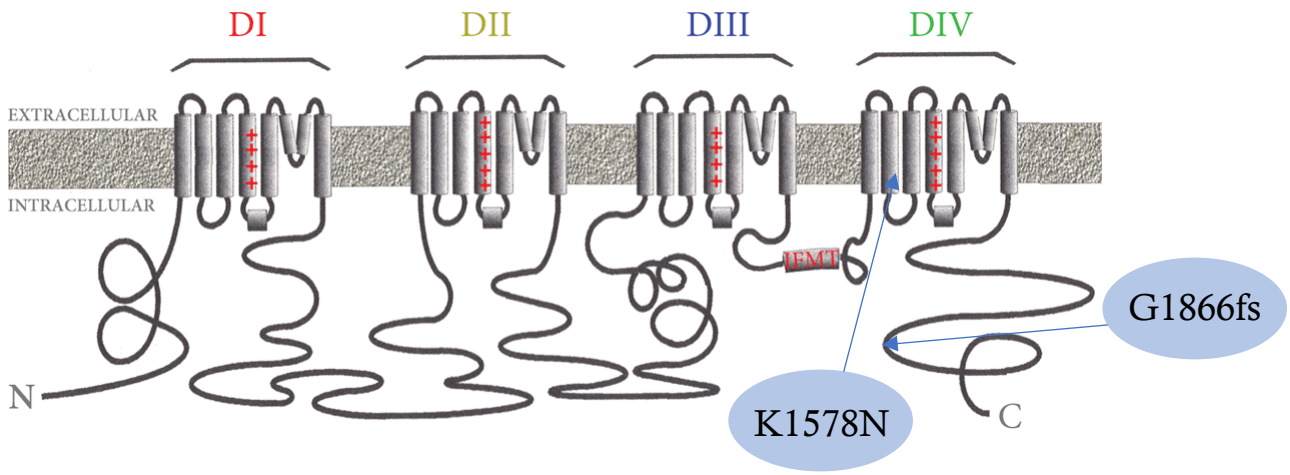

Figure 18. Schematic representation of Nav1.5 protein that shows the localization of both mutations

Considering the severe phenotype shown by the patient, computer analysis via SIFT was not used to verify the potential effect of the mutation. As we did in the previous part of the thesis, we started to evaluate the possible effect of the compound mutations on current density (**Figure 19**). We performed heterologous transient transfections of adult SCN5A in the Wild-Type (WT), p K1578N, and m G1866fs conditions on Human Embryonic Kidney cells (HEK 293). The same model was used for studying the compound neonatal K1578N7G1866fs. Panel A shows representative traces and panel B the current voltage plot. Compared to the WT, the maternal

heterozygous mutation m1866 shows a peak current density reduction of about 25%, while the paternal p1578 is decreased by about 40%, and the compound Neo1866/1578 shows a reduction of 60%. (Mean peak current densities: WT -118.1±10.2 pA/pF, n=42; m1866 -89.5±11.9 pA/pF, n=20; p1578 -68.3±11.3 pA/pF, n=21; Neo1866/1578 -38.3± 5.8 pA/pF, n=25. * P<0.05 at -20 mV).

Although the parents present a quite consistent reduction in the sodium current, they do not present any pathological phenotype. This could be due to compensatory mechanisms that make up for this reduction.

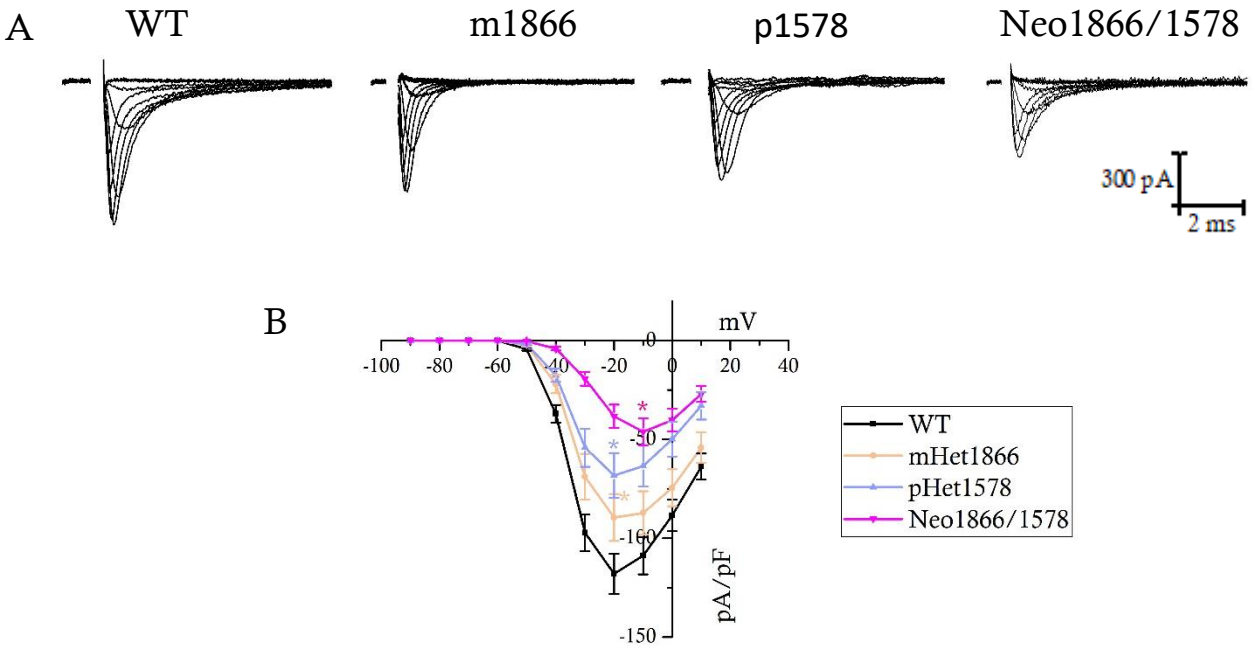

Figure 19. Effect of both mutations on current density.
A) Representative current traces recorded in GFP-positive HEK cells transfected with WT, WT/G1866fs (m1866), WT/K1578N (p1578), and neonatal G1866fs/K1578N (Neo1866/1578) hNav 1.5 cDNA. (B) Mean I-V curves, normalized to cell capacitance.

The results obtained in this first type of experiments suggested to keep on investigating the role of the compound mutations. Furthermore, looking at panel B we can appreciate the presence fof shift toward more positive potential of theI/V relation-(from -20 mV to -10 mV).

Then, we analyzed the voltage-dependence of activation and inactivation curves (**Figure 20**): m1866 and p1857 conditions did not induce any changes in the activation and inactivation curves, while the Neo1866/1578 significantly shifted the activation curve toward more depolarized voltages by about 9 mV and the inactivation by 5 mV (V½ activation, WT -30.8±0.4 mV, n=42; m1866 -28.4±0.4 mV, n=20; p1578 -29.8±0.3 mV, n=21; Neo1866/1578 -21.7±0.3

We considered that the positive shift of the inactivation curve should, by itself, increase the Neo1866/1578 current compared to WT, and this should counterbalance the peak current density reduction, observed before. The shift of the activation curve probably suggests a strong modification in the time constant of activation, but more analyses are required to confirm this evidence.

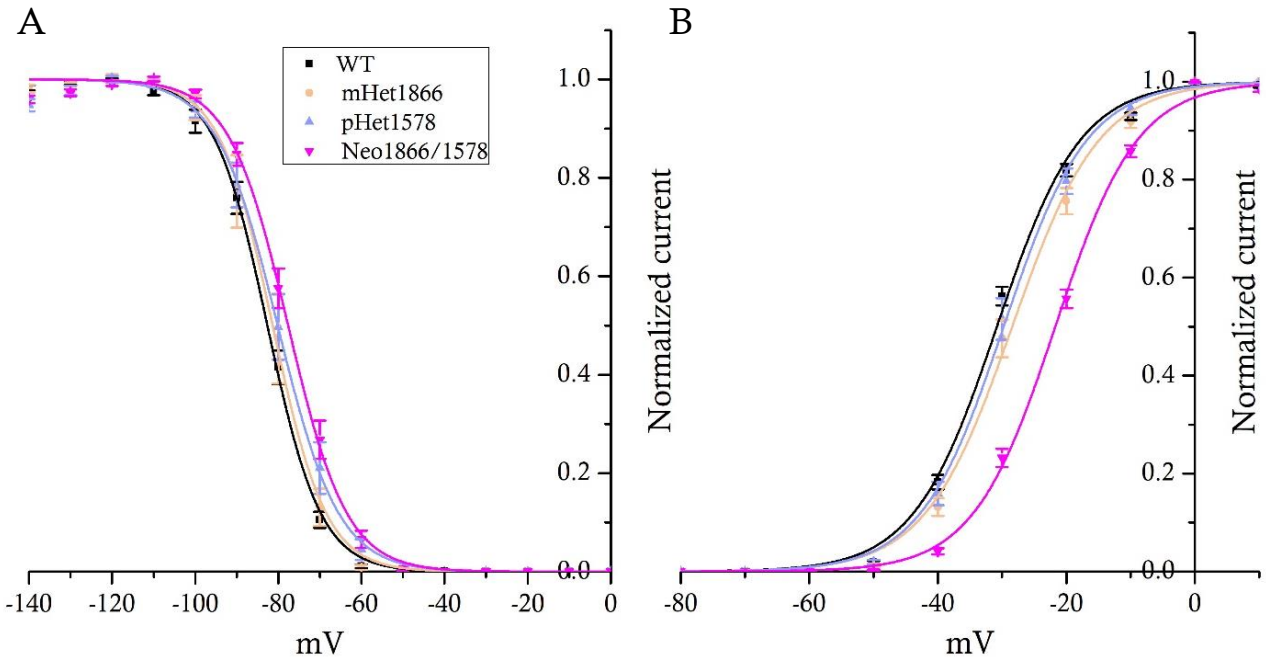

Figure 20. Neo1866/1578 mutation induces changes in the voltage-dependence of activation and inactivation.
(A) Mean inactivation curves obtained from WT, m1866, p1578, and Neo1866/1578 channels. Only Neo1866/1578 inactivation curve is positively shift by 5 mV. (B) Mean activation curves of WT, m1866, p1578, and Neo1866/1578 channels. The activation curve obtained in Neo1866/1578 condition is positively shifted by 9.1 mV.

We are aware that, regarding this project, other experiments will be needed to try to better delineate the situation and to explain the complex phenotype of the patient.

DISCUSSION

We need to be very careful about the procedures that we used when we are dealing with pediatric patient, especially in cases like this in which there is an overlap of different pathologies: sinus node dysfunction and atrial flutter due to genetic mutations carried by the baby and long-QT syndrome provoked by drugs administration. So, the clinical profile is not limited to SAN dysfunction (DeFilippo et al., 2015).

We decided to carry out this study using the neonatal isoform of the cardiac sodium channel which, unlike the adult form, differs in 7 amino acids present in exon 6: this is due to alternative splicing reasons. Our choice fell on the neonatal isoform of the channel, taking into account the age of the patient. Murphy et al., 2012 showed that the ratio neonatal versus adult decreases with aging, but we still do not know when the switch between isoforms take place during the development.

We started to evaluate the effect of the compound heterozygosity for paternal K1578N and maternal G1866fs (**Figure 19**): Neo1866/1578 induced a strong peak current density reduction of about 60%, confirming the severe phenotype of the patient. So, the compound heterozygosity acts as a loss-of-function mutation.

Although we also observed a current density reduction in both mutations carried by the parents (25% for maternal and 40% for paternal proband), they were totally asymptomatic, and they seemed to be healthy. We do not know the reason of their phenotypes, there are probably compensatory mechanisms that prevent the appearance of the symptoms.

The kinetic parameters analysis (**Figure 20**) showed that no changes in voltage-dependence of activation/inactivation are present in both mutations carried by the parents, while the son has strong alterations of both. In particular, we found a positive 5 mV shift of the inactivation curve and a positive 9 mV shift of the activation curve that dramatically altered the biophysical properties of the mutated channel.

Here, we have raised two fundamental points which are: i) the presence/absence of Na channels in the SAN and ii) the differential role that NAv1.5 mutations play in conduction tissue and/or in working myocytes

Voltage-gated sodium channels are typically expressed in the working myocardium while the presence in Sinoatrial node (SAN) has long been a debated issue. However, there are several evidences about the presence of NaV1.5 in different animal models (Baruscotti et al., 1996; Remme et al., 2009). In human primary SAN cells molecular biology experiments revealed that

NaV1.5 is poor (Chandler et al., 2009), but Werkerk and collaborators were capable to record sodium current in a single human SAN cells, proposing as a hypothesis that Nav1.5 was not present in the center of the SAN, but in the periphery (Werkerk et al., 2009). Despite the lack of Nav1.5 channels in primary pacemaker cells, there is ample evidence that many SCN5A mutations are associated with inherited SAN dysfunction manifestations such as bradycardia and sinus-exit block and that symptomatic and asymptomatic sinus bradycardia is also often observed both in patients affected by Brugada or LQT3 syndrome (Makita et al., 2007; Holst et al., 2010; Horn et al., 2011).

Sinus bradycardia could occur because of either a slower diastolic depolarization or an increased duration of the action potential. In vitro characterization of biophysical defects of Na^+ channels associated with cardiac rate slowing indicates that loss-of-function mutations (typical of Brugada syndrome) are responsible for a slower diastolic depolarization, while gain-of-function mutations (typical of LQT3 syndrome) are responsible for the longer duration of the action potential due to the presence of a non-inactivating sodium current component (Veldkamp et al., 2003; Lei et al., 2008).

Another group of researchers have investigated the effect of loss-of function Nav1.5 channel mutations by generating a mathematical model of the electrical activity of both isolated SAN cells and SAN-atrium two-dimensional preparation (Butters et al., 2010). These experiments confirmed that at the single cell level only peripheral cells are affected, but in the SAN-atrium simulation the model reproduced a slowing of both SAN rate and impulse conduction leading to SAN exit block or arrest. This study thus provides the rationale that supports the observation that mutations of the hNav1.5 channel are associated with clinical features typical of SAN dysfunction.

The above details robustly provide the logical/molecular interpretation of the association between SAN disease and Nav1.5 channel mutations. It is however a still challenging issue why some Nav1.5 mutation exert stronger pathological features in conduction tissue rather than working myocytes. At present there is evidence of a genetic association between ion channel mutations and atrial flutter therefore, it is highly speculative to hypothesize a cause-effect relation between the compound mutations observed in our proband and the phenotypic occurrence of AFL. Furthermore, at least to the level of investigations that has been clinically carried out so far, there is also no evidence of a slowing of the conduction impulse. This is all we did in the last months of my Ph.D and we know that there still is a lot of work to do in order to better understand this case-specific situation.

GENERAL CONCLUSIONS

In the two studies I presented in my thesis I want to highlight the importance of investigating the hereditary arrhythmias caused by ion channels, and accessory proteins' mutations, the so-called channelopathies. The study and identification of these diseases is very complicated because, in many cases, the first manifestation of the pathology coincides with the death of the individual.

The aim of our research is to understand the pathophysiological mechanisms at the molecular level in order to identify markers that allows us to prevent the triggering event of the pathology. In the specific case of my thesis, the first project, that I have been involved, gives us some new findings that may help explaining how and why Brugada syndrome takes place in a specific pathogenic environment. The new evidence I report in my research can be an additional piece to be added to the knowledge acquired so far about the physiological and molecular mechanism involved in BrS, and from which it is possible to start for future consideration in-depth research in the field of complex diseases such as cardiac channelopathies.

The second study starts from a case-report of a young patient affected by a strange case of overlap syndrome in which we are trying to elucidate some inherited aspects of the pathology. It is a project that recently started, but it is immediately giving us important and interesting results. Knowing the phenomena that underlie the pathology will surely help us to improve the patient's health care and lifestyle.

Limitations of experimental models used

When compared to other methodologies, the heterologous system clearly displays some limitations. For example, expression in HEK293 cells does not provide a cardiac cellular background to expression studies of Nav1.5 channel, and in this respect the possibility to use cardiomyocytes derived from iPCS would be a better choice. However as long as the purpose of the study is to identify differences in the biophysical features of mutant vs WT channel this method is well accepted and from an historical point it has been largely used. In addition, there are two other issues that have to be considered: firstly, the ease in keeping them in culture at a relatively low cost; secondly, the heterologous expression cell types often express a limited number of endogenous ion channels and this facilitates the electrophysiological study of channel proteins.

Last but not the least is the evidence that results collected using heterologous expression system always provide information that can be reliably translated to real phsyiolgical/pathological mechanisms.

MATERIALS AND METHODS

Cell culture

Human Embryonic Kidney 293 cells (HEK293) were used for evaluating the biophysical properties of the mutated channels. These cells represent a widely used cellular system in electrophysiology because they show reduced expression levels of ion channels and consequently, they present relatively small endogenous currents. They were cultured in DMEM (Dulbecco's Modified Eagle's Medium, Life Technology) supplemented with 10% FBS (Fetal Bovine Serum, Life Technology), 1% sodium pyruvate (S8636 Sigma-Aldrich), the 1% of L-Glutamine (Sigma-Aldrich), 0.5% of Penicillin and 0.5% of Streptomycin (0.1 mg / mL and 100 U / mL, Sigma-Aldrich, respectively). The cells were kept in a 37 ° C incubator with 5% CO_2.

Ventricular cardiomyocytes

Guinea pig ventricular cells were isolated using a retrograde coronary perfusion method similar to Langendorff heart. All procedures performed were in accordance with the Italian DL. 26/2014 and the European directive 2010/63/UE, regarding the protection of animals used for experimental and other scientific purposes. Animals were sacrificed by cervical dislocation under ketamine/xylazine (50 and 5 mg/kg, Sigma-Aldrich) anesthesia. Hearts were quickly removed, and the ascending aorta was connected to the outlet of a Langendorff column, perfused with Tyrode solution at 37°C, containing (mmol/L): NaCl 143, KCl 5.4, $CaCl_2$ 1.8, $MgCl_2$ 0.5, Hepes-NaOH 5, and D-glucose 5.5, adjusted to pH 7.4 with NaOH. Perfusion with Tyrode solution was maintained until vigorous mechanical activity resumed and blood was completely removed. The heart was them perfused, until arrest occurred, with 10 ml of enzymatic solution, containing: Tyrode, liberase 0.1mg/ml and BSA (Sigma-Aldrich) 1mg/ml, $CaCl_2$ 12.5µM, trypsin-EDTA solution (Sigma-Aldrich) 0.02 mg/ml. When the effluent became viscous, the heart was moved to a Ca^{2+}-free solution (0.1mmol/L EGTA added), and the right ventricle outflow tract was isolated and chopped in fragments. The fragments were exposed to gentle mechanical agitation in Ca^{2+}-free solution. The solution was recovered, filtered through a nylon mesh, and centrifuged at 750rpm for 3 minutes. The pellet was resuspended in Ca^{2+}-free solution and stored at 4°C until use.

Plasmids and transfection

The adult human (h) SCN5A WT (NM_000335.4) in pcDNA1.1 vector was gently given by Flavien Charpientier and the S805L mutation (Serine TCG > Leucine TTG) was introduced through a site-directed mutagenesis kit (*QuikChange II XL Site-Directed Mutagenesis Kit,* Agilent Technologies) using the following primers: F 5' -tgtcccgcatgagcaacttgttggtgctgcgctccttc-3', R 5' -gaaggagcgcagcaccaacaagttgctcatgcgggaca-3'.

The neonatal (Neo) human SCN5A (NM_001099404.1) in pcDNA1.1 was used to study the compound mutation found by our collaborators in Bergamo in a younger patient. This variant differs from the adult in exon 6 because of alternative splicing. In particular, there are 7 aminoacidic modifications compared to the adult form of the channel: T206V, T207S, F209N. V210I, D211K, V215L, and S234P. Also, in this case the mutations K1578N and G1866fs were introduce through the same kit, using the following primers: F 5'-cacaggcgagtgtattgtcaacctggctgccctgc-3' and R 5' -gcagggcagccaggttgacaatacactcgcctgtg- 3' for the K1578N and F 5' – tcctgggggagtcagtctggggagatggac- 3' R 5' -gtccatctccccagactgactcccccagga- 3' for the G1866fs.

Automated DNA sequence analysis (BioFab Research, Italy) was used to verify the mutation.

HEK293 cells plated on 35-mm dishes were transfected for functional expression with 1 μg of expression vector containing the accessory β-subunit protein SCN1B and Green Fluorescent Protein (GFP), and 1 μg of either WT or S805L hSCN5A or with 0.5 μg of both using *ViaFect™* (Promega). The transfection of the same quantity of WT and S805L plasmids was done in order to simulate the heterozygous condition of the patients. Regarding the mutation found in the young patient, we transfected HEK293 cells with 1 μg of expression vector containing the accessory β-subunit protein SCN1B and Green Fluorescent Protein (GFP), and 1 μg of WT, or 1 μg Neo G1866fs/K1578N or with 0.5 μg of WT and G1866fs to mimic the maternal form of the channel or 0.5 μg of WT and 0.5 μg K1578N to analyze the paternal one, using *ViaFect™* (Promega). The transfection of the same quantity of WT and G1866fs or WT and K1578N plasmids were done in order to simulate the heterozygous condition of the parents.

Electrophysiological setup

The standard electrophysiological setup is composed by:

- an inverted microscope (Axiovert S100) settled on a vibrating-damping table;
- an analog/digital interface (Digidata 1550B, Axon Instruments);

- a microelectrode amplifier (Axopatch 200B, Axon Instruments);
- an amplifier head stage (CV-203BU, Axon Instruments);
- a mechanical micromanipulator;
- a temperature control system;
- a standard PC workstation with pClamp 10.7 software (Molecular Devices, LCC).

All these devices are boxed in a Faraday cage in order to isolate the setup from external electrical noises.

Patch-clamp procedures

Electrophysiological experiments were performed using the patch-clamp technique in whole-cell configuration. The day after the transfection, the cells were dispersed by trypsin-EDTA and plated at low density on 35-mm plastic petri dishes, in order to record sodium currents from single cells. The following day, GFP-expressing cells were selected for patch-clamp analysis. HEK 293 cells were maintained at room temperature (25 °C), while guinea pig ventricular cardiomyocytes were kept at 36±1°C. HEK 293 cells were kept in Tyrode's solution containing (mM): NaCl 140, KCl 5.4, $CaCl_2$ 1.8, D-glucose 5.5 and Hepes 5, pH 7.4. Ventricular cardiomyocytes were initially maintained in another physiological solution containing different ions concentrations (mM): NaCl 154, KCl 4, $CaCl_2$ 2, $MgCl_2$ 1, Hepes-NaOH 5, D-glucose 5.5, adjusted to pH 7.35. In HEK 293 cells, the SCN5A current was recorded in a low sodium external solution containing (mM): NMDG-Cl 100, NaCl 30, CsCl 5, Hepes 10, $MgCl_2$ 1.2, $CaCl_2$ 2 and Glucose 5, pH 7.4. Late sodium current from HEK 293 cells was dissected by adding Tetrodotoxin citrate (TTX, HelloBio) to low sodium external solution.

In order to record sodium currents, patch-clamp pipettes, pulled from borosilicate glass capillaries, had a resistance of 2-2.5 MΩ and filled with an internal solution containing (mM): CsCl 130, NaCl 10, $MgCl_2$ 1, Hepes 10, EGTA 10, Na $_2$ATP 2, pH 7.2. For recordings in ventricular myocytes, pipettes had a resistance of 4-7 MΩ and were filled with an intracellular-like solution containing (mM): K-Aspartate, 130; NaCl, 10; EGTA-KOH, 5; CaCl2, 2; MgCl2, 2; ATP (Na-salt), 2; creatine phosphate, 5; GTP (Na-salt), 0.1; pH 7.2.

All Na^+ current traces were low pass filtered at a frequency of 10 kHz and the sampling rate was set at 20 μs. Activation curve of sodium current was elicited by depolarizing voltages steps from -90 mV to +10 mV, and cells were maintained at a holding potential (hp) of -120 mV, -100mV, and -80 mV. Inactivation curves were obtained by maintaining cells at holding potential of -100

mV and giving depolarizing steps from -140 mV to 0 mV of 1 s of duration. To obtain smooth curves, the data were fitted according to Boltzmann equation: $Y = 1/(1 + \exp((V - V_{1/2})/s))$ for inactivation and $Y = 1/(1 + \exp(-(V - V_{1/2})/s))$ for the activation, where y is the fractional activation, V is the voltage, $V_{1/2}$ is the half-activation voltage, and s is the inverse of the slope factor.

Current density is defined as the amount of electric current per unit of cross section and it's measured in pA/pF. SCN5A current density was obtained from current amplitude at each step potential normalized to cell capacitance.

The recovery from inactivation was obtained by a double pulse protocol. Cells were depolarized to 0 mV for 50 ms from a holding potential of -120 mV, then returned to the holding potential with an interval from 0.4 to 13.2 s and a second step of 50 ms to 0 mV was then delivered. Late sodium current, as TTX-sensitive, was recorded using a repeated protocol of a single depolarized step from a holding potential of -120 mV to -20 mV. Time constants were calculated by fitting the activation current traces with a mono-exponential function.

Action potentials of guinea pig ventricular myocytes were recorded in current-clamp mode at a sampling rate of 2 KHz and filtered at 5 KHz with pClamp software by depolarizing current steps up to 10 pA.

Data analysis and statistics

Protocols were designed using pClamp 10.7 and data were also acquired with the same software. Data were analyzed with Clampfit and Origin 2016. All results are presented as average ± standard error of the average (SEM); the statistical tests used are t tests for coupled values and ANOVA tests. Statistical significance was set at $P < 0.05$.

REFERENCES

Abriel H., Rougier J. S. & Jalife J. Ion Channel Macromolecular Complexes in Cardiomyocytes: Roles in Sudden Cardiac Death. *Circulation Research*; 116(12): 1971–1988, **2015**.*Ann N Y Acad Sci.* Mar; 1123:213-23, **2008**.

Antzelevitch C., Yan G. X. & Shimizu W. The Brugada syndrome versus long-QT syndrome. *Journal of electrocardiology*, vol 32, **1999.**

Antzelevitch C. The Brugada Syndrome: Ionic Basis and Arrhythmia Mechanism**.** *Journal of Cardiovascular Electrophysiology*, Volume 12, No. 2, **2001**.

Ashpole N. M., Herren A. W., Ginsburg K. S., Brogan J. D., Johnson D. E., Cummins T. R.,Bers D. M. & Hudmon A. Ca2+/Calmodulin-dependent Protein Kinase II (CaMKII) regulates cardiac sodium channel NaV1.5 gating by multiple phosphorylation sites. *J Biol Chem* 287:19856–69; **2012**.

Balser J. R., Nuss H. B., Chiamvimonvat N., Pérez-García M. T., Marban E. & Tomaselli G. F. External pore residue mediates slow inactivation in mu 1 rat skeletal muscle sodium channels. *J Physiol.* Jul 15;494 (Pt 2):431-42, **1996**.

Barbuti A. & DiFrancesco D. Control of cardiac rate by "funny" channels in health and disease. *Ann N Y Acad Sci.* Mar1123:213-23, **2008**.

Baruscotti M. DiFrancesco D. & Robinson R. B. A TTX-sensitive inward sodium current contributes to spontaneous activity in newborn rabbit sino-atrial node cells. *The Journal of Physiology*, 492(Pt 1), 21–30, **1996**.

Beltran-Alvarez P., Pagans S. & Brugada R. The cardiac sodium channel is post-translationally modified by arginine methylation. *J Proteome Res* 10:3712–9; **2011**.

Beltran-Alvarez P., Espejo A., Schmauder R., Beltran C., Mrowka R., Linke T., Battle M., Pérez-Villa F., Pérez G. J., Scornik F. S., Benndorf K., Pagans S., Zimmer T & Brugada R. Protein arginine methyl transferases-3 and -5 increase cell surface expression of cardiac sodium channel. *FEBS Lett* 587:3159-65; **2013**.

Benito B., Brugada R., Brugada J. & Brugada P. Brugada syndrome. *Prog Cardiovasc Dis*.; 51:1–22, **2008**.

Benson D. W., Wang D. W., Dyment M., Knilans T. K., Fish F. A., Strieper M. J., Rhodes T. H. & George A. L. Jr. Congenital sick sinus syndrome caused by recessive mutations in the cardiac sodium channel gene (SCN5A). *J Clin Invest* 112:1019-1028, **2003**.

Berecki G., Zegers J. G., Bhuiyan Z. A., Verkerk A. O., Wilders R. & van Ginneken A. C. Long-QT syndrome-related sodium channel mutations probed by the dynamic action potential clamp technique. *J Physiol.* Jan 15;570(Pt 2):237-50, **2006**.

Berne P., Brugada J. Brugada syndrome. *Circ J*. 2012;76(7):1563-71, **2012**.

Bezzina C. R., Tan H. L. Pharmacological rescue of mutant ion channels. *Cardiovasc Res.*Aug 1;55(2):229-32, **2002**.

Black N., D'Souza A., Wang Y., Piggins H., Dobrzynski H., Morris G. & Boyett M. R. Circadian rhythm of cardiac electrophysiology, arrhythmogenesis, and the underlying mechanisms. *Heart Rhythm*. Feb;16(2):298-307, **2019**.

Brown H. F., DiFrancesco D. & Noble S. J. How does adrenaline accelerate the heart? *Nature* 280, 235-236, **1979**.

Brugada P. & Brugada J. Right bundle branch block, persistent ST segment elevation and sudden cardiac death: A distinct clincal and eletrocardiographic syndrome. *JACC* Vol. 20. N°6, 1391-6, **1992**.

Brugada P. Brugada syndrome: More than 20 years of scientific excitement. *Journal of Cardiology* 67 215–220, **2016**.

Brugada R., Campuzano O., Sarquella-Brugada G., Brugada J. & Brugada P., Brugada Syndrome. *Houston methodist debakey cardiovascular journal,* **2014**.

Bun S. S., Latcu D.G., Marchlinski F. & Saoudi N. Atrial flutter: more than just one of a kind. *Eur Heart J.* Sep 14;36(35):2356-63, **2015**.

Butters T. D., Aslanidi O. V., Inada S., Boyett M. R., Hancox J. C., Lei, M. & Zhang H. Mechanistic links between Na+ channel (SCN5A) mutations and impaired cardiac pacemaking in sick sinus syndrome. *Circulation Research*, 107(1), 126−137; **2010**.

Campuzano O., Brugada R. & Iglesias A. Genetics of Brugada syndrome. *Curr Opin Cardiol.* May;25(3):210-5, **2010**.

Catteral W. A. Molecular properties of voltage-sensitive sodium channels. *Annu Rev Biochem*; 55:953-85, **1986**.

Catterall W. A. From ionic currents to molecular review mechanisms: the structure and function of voltage-gated sodium channels. *Neuron*, Vol. 26, 13–25, **2000**.

Catterall W. A. Voltage-gated sodium channels at 60: structure, function and pathophysiology. *J Physiol* 590.11, 2577–2589, **2012**.

Chandler N. J., Greener, I. D., Tellez, J. O., Inada, S., Musa, H., Molenaar, P., Difrancesco D., Baruscotti M., Longhi R., Anderson R. H., Billeter R., Sharma V., Sigg D. C., Boyett M. R. & Dobrzynski H. Molecular architecture of the human sinus node: insights into the function of the cardiac pacemaker. *Circulation*, 119(12), 1562−1575; **2009.**

Choudhury M., Boyett M. R. & Morris M. G. Biology of the sinus node and its disease. *Arrhythmia & Electrophysiology Review.* 4(1):28–34, **2015**

Cosío F. G. Atrial Flutter, Typical and Atypical: A Review. *Arrhythm Electrophysiol Rev.* Jun;6(2):55-62, **2017**.

De Filippo P., Ferrari P., Iascone M., Racheli M. & Senni M. Cavotricuspid isthmus ablation and subcutaneous monitoring device implantation in a 2-year-old baby with 2 SCN5A mutations, sinus node dysfunctions, atrial flutter recurrences, and drug induced long-QT syndrome: a tricky case of pediatric overlap syndrome? *J Cardiovasc Electrophysiol* 26(3):346-9, **2015**.

Deschenes I., Neyroud N., DiSilvestre D., Marban E., Yue D. T. &Tomaselli G. F. Isoform-specific modulation of voltage-gated Na(+) channels by calmodulin. *Circ Res*; 90:E49–57, **2002.**

Di Diego J. M., Cordeiro J. M., Goodrow R. J., Fish J. M., Zygmunt A. C., Perez G. J., Scornik F. S. & Antzelevitch C. Ionic and cellular basis for the predominance of the Brugada syndrome phenotype in males. *Circulation* 106: 2004–11, **2002**.

DiFrancesco D. & Tortora P. Direct activation of cardiac pacemaker channels by intracellular cyclic AMP. *Nature* 351(6322), 145-147, **1991**.

DiFrancesco D., Ferroni A., Mazzanti M. & Tromba C. Properties of the hyperpolarizing-activated current (if) in cells isolated from the rabbit sino-atrial node. *The Journal of Physiology* 377, 61, **1986**.

Evans R. & Shaw D. Pathological studies in sinoatrial disorder (sick sinus syndrome). *Br Heart J* 39:778–86, **1977**.

Granada J., Uribe W., Chyou P. H., Maassen K., Vierkant R., Smith P. N., Hayes J., Eaker E. & Vidaillet H. Incidence and predictors of atrial flutter in the general population. *J. Am. Coll. Cardiol.* Dec;36(7):2242-6, **2000.**

Halligan S. C., Gersh B. J., Brown R. D., Rosales A. G., Munger T. M., Shen W. K., Hammill S. C. & Friedman P. A. The natural history of lone atrial flutter. *Ann. Intern. Med.* Feb 17;140(4):265-8, **2004**.

Heras M. & Fernàndez-Reyes M. J. Serum potassium concentrations: importance of normokalaemia. *Med Clin* (Barc) 21;148(2):562-565, **2017**.

Holst A. G., Liang, B., Jespersen, T., Bundgaard, H., Haunso, S., Svendsen, J. H. & Tfelt-Hansen J. Sick sinus syndrome, progressive cardiac conduction disease, atrial flutter and ventricular tachycardia caused by a novel SCN5A mutation. *Cardiology*, 115(4), 311− 316; **2010**.

Honjo H., Boyett M. R., Kodama I. & Toyama J. Correlation between electrical activity and the size of rabbit sino-atrial node cells. *The Journal of Physiology*, 496(Pt 3),795–808, **1996**.

Horne A. J., Eldstrom J., Sanatani S. & Fedida, D. A novel mechanism for LQT3 with 2:1 block: a pore-lining mutation in Nav1.5 significantly affects voltage-dependence of activation. *Heart Rhythm*, 8(5), 770−777; **2011**.

Huang W., Liu M., Yan F. S. & Yan N. Structure-based assessment of disease- related mutations in human voltage-gated sodium channels. *Protein Cell*, 8(6):401–438, **2017**.

Kall J. G., Rubenstein D. S., Kopp D. E., Burke M. C., Verdino R. J., Lin A. C., Johnson C. T., Cooke P. A., Wang Z. G., Fumo M. & Wilber D. J. Atypical atrial flutter originating in the right atrial free wall. *Circulation.* Jan 25;101(3):270-9, **2000**.

Kalman J. M., Olgin J. E., Saxon L. A., Lee R. J., Scheinman M. M. & Lesh M. D. Electrocardiographic and electrophysiologic characterization of atypical atrial flutter in man: use of activation and entrainment mapping and implications for catheter ablation. *J. Cardiovasc. Electrophysiol.* Feb;8(2):121-44, **1997**.

Kapplinger J. D., **Tester D. J.**, **Alders M.**, **Benito B.**, **Berthet M.**, **Brugada J.**, **Brugada P.**, **Fressart V.**, **Guerchicoff A.**, **Harris-Kerr C.**, **Kamakura S.**, **Kyndt F.**, **Koopmann T. T.**, **Miyamoto Y.**, **Pfeiffer R.**, **Pollevick G. D.**, **Probst V.**, **Zumhagen S.**, **Vatta M.**, **Towbin J. A.**, **Shimizu W.**, **Schulze-Bahr E.**, **Antzelevitch C.**, **Salisbury B. A.**, **Guicheney P.**, **Wilde A. A.**, **Brugada R.**, **Schott J. J. & Ackerman M. J**. An international compendium of mutations in the SCN5A-encoded cardiac sodium channel in patients referred for Brugada syndrome genetic testing. *Heart Rhythm*. Jan;7(1):33-46, **2010**.

Kaumann A. J. & Molenaar P. Modulation of human cardiac function through 4 β-adrenoceptor populations. *Naunyn-Schmiedeberg's archives of pharmacology* 355(6), 667-681, **1997**.

Kent K. M., Epstein S. E., Cooper T. & Jacobowitz D. M. Cholinergic innervation of the canine and human ventricular conducting system Anatomic and electrophysiologic correlations. *Circulation* 50(5), 948-955, **1974**.

Klein G. J., Guiraudon G. M., Sharma A. D. & Milstein S. Demonstration of macroreentry and feasibility of operative therapy in the common type of atrial flutter. *Am. J. Cardiol.* Mar 01;57(8):587-91, **1986**.

Lei M., Huang C. L., & Zhang, Y. Genetic Na+ channelopathies and sinus node dysfunction. *Progress in Biophysics and Molecular Biology*, 98(2−3), 171−178; **2008**.

Light P. E., Wallace C. H. & Dyck J. R. Constitutively active adenosine monophosphate-activated protein kinase regulates voltage-gated sodium channels in ventricular myocytes. *Circulation* 107:1962–5; **2003**.

Lu Z., Wu C. Y., Jiang Y. P., Ballou L. M., Clausen C., Cohen I. S. & Lin R. Z. Suppression of phosphoinositide 3-kinase signaling and alteration of multiple ion currents in drug induced long QT syndrome. *Sci Transl Med* 4 (131ra50); **2012**.

Makielsky J. C., Ye B., Valdivia C. R., Pagel M. D., Pu J., Tester D. J. & Ackerman M. J. A ubiquitous splice variant and common polymorphism affect heterologous expression of recombinant human SCN5A heart sodium channels. *Circ Res.* 31;93(9):821-8, **2003**.

Makita N., Sumitomo, N., Watanabe, I., & Tsutsui, H. Novel SCN5A mutation (Q55X) associated with age-dependent expression of Brugada syndrome presenting as neurally mediated syncope. *Heart Rhythm*, 4(4), 516−519; **2007**.

Marionneau C. & Abriel H. Regulation of the cardiac Na^+ channel $Na_V1.5$ by post-translational modifications. *Journal of Molecular and Cellular Cardiology* 82 36-47, **2015**.

Mercier A., Clèment R., Harnois T., Bourmeyster N., Bois P. & Chatelier A. $Na_v1.5$ channels can reach the plasma membrane through distinct N-glycosylation states. *Biochimica et Biophysica Acta* 1850 (1215-1223), **2015**.

Meregalli P. G., Wilde A. A. & Tan H. L. Pathophysiological mechanisms of Brugada syndrome: depolarization disorder, repolarization disorder, or more? *Cardiovasc Res* 67:367–78, **2005**.

Milanesi R., Bucchi A. & Baruscotti M. The genetic basis for inherited forms of sinoatrial dysfunction and atrioventricular node dysfunction. *Interv Card Electrophysiol* 43:121–134, **2015**.

Mittal S., Pokushalov E., Romanov A., Ferrara M., Arshad A., Musat D., Preminger M., Sichrovsky T. & Steinberg J. S. Long-term ECG monitoring using an implantable loop recorder for the detection of atrial fibrillation after cavotricuspid isthmus ablation in patients with atrial flutter. *Heart Rhythm.* Nov;10(11):1598-604, **2013**.

Morris G. M. & Kalman J. M. Fibrosis, electrics and genetics. Perspectives in sinoatrial node disease. *Circ J* 78:1272–82, **2014**.

Murphy B. J., Rogers J., Perdichizzi A. P., Colvin A. A. & Catteral W. A. cAMP-dependent phosphorylation of two sites in the alpha subunit of the cardiac sodium channel. *J Biol Chem* 271:28837-43; **1996.**

Murphy L. L., Moon-Grady A. J., Cuneo B. F., Wakai R. T., Yu S., Kunic D. J., Benson D. W. & George A. L. Jr. Developmentally Regulated *SCN5A* Splice Variant Potentiates Dysfunction of a Novel Mutation Associated with Severe Fetal Arrhythmia. *Heart Rhythm.* April 9(4): 590–597, **2012**.

Nademanee K. L., Veerakul G., Chandanamattha P., Chaothawee L., Ariyachaipanich A., Jirasirirojanakorn K., Likittanasombat K., Bhuripanyo K. & Ngarmukos T. Prevention of ventricular fibrillation episodes in Brugada syndrome by catheter ablation over the anterior right ventricular outflow tract epicardium. *Circulation.* Mar 29;123(12):1270-9, **2011**.

Nava A., Canciani B., Martini B. & Buja G. F. La ripolarizzazione precoce nelle precordiali destre. Correlazioni ECG-VCG elettrofisiologia. *Giornale italiano di cardiologia* 18 (suppl 1):118, **1988**.

Naccarelli G. V., Varker H., Lin J. & Schulman K. L. Increasing prevalence of atrial fibrillation and flutter in the United States. *Am J Cardiol.* Dec 1;104(11):1534-9, **2009.**

Nerbonne J. M. & Kass R. S. Molecular physiology of cardiac repolarization. *Physiological Reviews* 85(4), 1205-53. Review, **2005**.

Pappone C., Brugada J., Vicedomini G., Ciconte G., Manguso F., Saviano M., Vitale R., Cuko A., Giannelli L., Calovic Z., Conti M., Pozzi P., Natalizia A., Crisà S., Borrelli V., Brugada R., Sarquella-Brugada G., Guazzi M., Frigiola A., Menicanti L. & Santinelli V. Electrical substrate elimination in 135 consecutive Brugada Syndrome patients. *Circ Arrhythm Electrophysiol*, 10, **2017**.

Polovina M. M., Vukicevic M., Banko B., Lip G. Y. H. & Potpara S. T Brugada syndrome: A general cardiologist's perspective. *European Journal of Internal Medicine*, **2017**.

Qu Y., Rogers J., Tanada T., Scheuer T. & Catterall W. A. Modulation of cardiac Na+ channels expressed in a mammalian cell line and in ventricular myocytes by protein kinase C. *Proc Natl Acad Sci U S A* 91:3289–93; **1994**.

Remme C. A., Verkerk A. O., Hoogaars W. M., Aanhaanen W. T., Scicluna B. P., Annink C., van den Hoff M. J., Wilde A.A., van Veen T. A., Veldkamp M. W., de Bakker J. M., Christoffels V. M. & Bezzina C. R. The cardiac sodium channel displays differential distribution in the conduction system and transmural heterogeneity in the murine ventricular myocardium. *Basic Research in Cardiology,* 104(5), 511–522, **2009**.

Rodriguez Ziccardi M., Goyal A. & Maani C. V. Atrial flutter. *StatPearls, Treasure Island* (FL), **2019**.

Rook B. M., Evers M. M., Vos M. A. & Bierhuizen M. F. A. Biology of cardiac sodium channel Nav1.5 expression. *Cardiovascular Research* 93, 12–23, **2012**.

Ruan Y., Liu N. & Priori S. G. Sodium channel mutations and arrhythmias. *Nat Rev Cardiol.* 2009 May;6(5):337-48, **2009**.

Schroder E. A., Lefta M., Zhang X., Bartos D. C., Feng H. Z., Zhao Y., Patwardhan A. Jin J. P., Esser K. A. & Delisle B. P. The cardiomyocyte molecular clock, regulation of *Scn5a*, and arrhythmia susceptibility *Am J Physiol Cell Physiol* 304: C954–C965, 2013.

Sendfeld F., Selga E., Scornik F. S., Perez G. J., Mills N. L. & Brugada R. Experimental models of Brugada syndrome. *Int J Mol Sci*. May;20(9):2123, **2019.**

Sodeck G. H., Domanovits H., Meron G., Rauscha F., Losert H., Thalmann M., Vlcek M. & Laggner A. N. Compromising bradycardia: management in the emergency department. *Resuscitation.* 73:96–102, **2007**.

Sunami A., Fan Z., Nakamura F., Naka M., Tanaka T., Sawanobori T. & Hiraoka M. The catalytic subunit of cyclic AMP-dependent protein kinase directly inhibits sodium channel activities in guinea-pig ventricular myocytes. *Pflugers Arch* 72:807-15; **1991**.

Tai C. T. & Chen S. A. Electrophysiological mechanisms of atrial flutter. *J Chin Med Assoc.* Feb;72(2):60-7, **2009**.

Thery C., Gosselin B., Lekieffre J. & Warembourg H. Pathology of sinoatrial node. Correlations with electrocardiographic findings in 111 patients. *Am Heart J* 93:735–40, **1977**.

Tukkie R., Sogaard P., Vleugels J., de Groot I. K., Wilde A. A. & Tan H. L. Delay in right ventricular activation contributes to Brugada syndrome. *Circulation* 109:1272 –7, **2004**.

Valdivia C. R., Ackerman M. J., Tester D. J., Wada T., McCormack J., Ye B. & Makielski J. C. A novel SCN5A arrhythmia mutation, M1766L, with expression defect rescued by mexiletine. *Cardiovasc Res*.Aug 1;55(2):279-89, **2002**.

Valdivia C. R., Tester D. J., Rok B. A., Porter C. B., Munger T. M., Jahangir A., Makielski J. C. & Ackerman M. J. A trafficking defective, Brugada syndrome-causing SCN5A mutation rescued by drugs. *Cardiovasc Res.* Apr 1;62(1):53-62, **2004**.

Veerman C. C., Wilde A. A. M. & Lodder E. M. The cardiac sodium channel gene SCN5A and its gene product Nav1.5: Role in physiology and pathophysiology. *Gene* 573:177–187, **2015**.

Veldkamp M. W., Wilders R., Baartscheer A., Zegers J. G., Bezzina C. R., & Wilde A. A. Contribution of sodium channel mutations to bradycardia and sinus node dysfunction in LQT3 families. *Circulation Research*, 92(9), 976−983; **2003**.

Wagner S., Dybkova N., Rasenack E. C., Jacobshagen C., Fabritz L., Kirchhof P. Maier S. K., Zhang T., Hasenfuss G., Brown J. H., Bers D. M & Maier L. S. Ca2+/calmodulin-dependent protein kinase II regulates cardiac Na+ channels. *J Clin Invest* 116:3127–38; **2006.**

Waldo A. L. & Feld G. K. Inter-relationships of atrial fibrillation and atrial flutter mechanisms and clinical implications. *J Am Coll Cardiol.* Feb 26;51(8):779-86, **2008.**

Walsh D. A. & Van Patten S. M. Multiple pathway signal transduction by the cAMP-dependent protein kinase. *The FASEB Journal* 8(15), 1227-1236, **1994**.

Watanabe H. & Minamino T. Genetics of Brugada syndrome. *J Hum Genet.* Jan;61(1):57-60, **2016**.

Verkerk, A. O., Wilders, R., van Borren, M. M., & Tan, H. L. Is sodium current present in human sinoatrial node cells? *International Journal of Biological Sciences*, 5(2), 201−204; **2009.**

Yan G. X. & Antzelevitch C. Cellular basis for the Brugada syndrome and other mechanisms of arrhythmogenesis associated with ST-segment elevation. *Circulation.* Oct 12;100(15):1660-6, **1999**.

Zhao Y., Scheuer T. & Catterall W. A. Reversed voltage-dependent gating of a bacterial sodium channel with proline substitutions in the S6 transmembrane segment. *Proc Natl Acad Sci U S A*; 101:17873–17878, **2004**.

Zhou J., Yi J., Hu N., George Jr. A. L. & Murray K. T. Activation of protein kinase a modulates trafficking of human cardiac sodium channel in xenopus oocytes. *Circ Res* 87:33-8, **2000.**